NATIONAL ADVISORY COMMITTEE FOR AERONAUTICS

TECHNICAL MEMORANDUM 1363

A NEW SIMPLE INTERFEROMETER FOR OBTAINING QUANTITATIVELY EVALUABLE FLOW PATTERNS

By S. F. Erdmann

Translation of "Ein Neues, Sehr Einfaches Interferometer zum Erhalt Quantitativ Auswertbarer Strömungsbilder."
Appl. Sci. Research, vol. B 2.

Washington
November 1953

1R

NATIONAL ADVISORY COMMITTEE FOR AERONAUTICS

TECHNICAL MEMORANDUM 1363

A NEW SIMPLE INTERFEROMETER FOR OBTAINING QUANTITATIVELY EVALUABLE FLOW PATTERNS*

By S. F. Erdmann

SUMMARY

The method described in the present report makes it possible to obtain interferometer records with the aid of any one of the available schlieren optics by the addition of very simple expedients, which fundamentally need not be inferior to those obtained by other methods, such as the Mach-Zehnder interferometer, for example. The method is based on the fundamental concept of the phase-contrast process developed by Zernike, but which in principle has been enlarged to such an extent that it practically represents an independent interference method for general applications. Moreover, the method offers the possibility, in case of necessity, of superposing any apparent wedge field on the density field to be gaged, hence to produce more favorable evaluation conditions and greater accuracy.

The theory is explained on a purely physical basis and illustrated and proved by experimental data. A number of typical cases are cited and some quantitative results reported.

It was found that this development reacts comparatively little to disturbing acoustic or mechanical oscillations. This is probably due to the fact that the two light beams causing the interferences are not separated until immediately before photographing and up to that point are subjected to the same effects. As regards the special possibilities which eventually might result with the use of white light and the use of auxiliary cameras, no systematic investigations have as yet been made.

1. INTRODUCTION

Interest in interferometry for the visualization and the quantitative evaluation of air flows at high subsonic and supersonic speeds has increased considerably within the last few years. This holds true for almost all laboratories which earlier were contented with schlieren

---

*"Ein Neues, Sehr Einfaches Interferometer zum Erhalt Quantitativ Auswertbarer Strömungsbilder." Appl. Sci. Research, vol. B 2.

photographs. The Mach-Zehnder interferometer has itself proved to be very expensive, especially for comparatively great images and hence frequently as exorbitant. Furthermore, it is very receptive to outside disturbances, especially to mechanical and acoustic oscillations, and, when used in combination with the necessarily very careful adjustment, is so difficult that highly trained personnel are required to operate it. These drawbacks do not exist in the present method and its possibilities are little if at all inferior to those of the Mach-Zehnder interferometer in the majority of uses coming into question. This new method in its present enlarged form makes it possible to change any schlieren apparatus into an interferometer by a few manipulations and a minimum of auxiliary equipment. The only fundamental drawback of the method compared to the Mach-Zehnder interferometer lies in a relatively very poor light output. But this need not signify a difficulty in principle if the flow to be studied is itself sufficiently steady.

The method to be described here is a considerably extended elaboration of the phase-contrast method suggested by Zernike in microscopy and so successfully used in the study of astronomic mirrors (refs. 1 to 5). The suggestion of investigating the suitability of this method for quantitative studies of flows is due to Professor Burgers of Delft.

The principle of the described method is based largely upon the fact that a certain part of the light passing through the plane of the object experiences a special treatment in the plane of the light source image, so that this light, in unison with the other unaffected light, produces interferences in the plane of the object image. Under certain assumptions, the thus produced interference figure gives a true reproduction of the existing density field, by showing lines of equal density (similar to the Mach-Zehnder setting for infinite band width), or apparent density fields of constant gradients, termed wedge fields hereafter, can be superposed (similar to the band fields of the Mach-Zehnder interferometer), or linear systems of bands of equal density increase in a certain direction referred to a variable level can occur, for which the Mach-Zehnder interferometer knows no analogue. The fact that the separation of the last interfering light beams takes place immediately before the picture is formed, ensures that this method is scarcely more receptive to outside disturbances than any sensitive schlieren apparatus.

The aim of Zernike's phase-contrast method consists in rendering minute phase differences even of small fractions of a wave length, caused by an object, visible, and not by forming bands, that is, black-white effects, but by differences in brightness (contrast). Even phase fluctuations can be identified and even measured if necessary, which normal interferometers no longer indicate. It can also be used to phase differences of several wave lengths when pronounced fields of disturbance are involved, that is, when small areas of greatly changed phase are present in a relatively great field of undisturbed light. However, the

method fails when the strong disturbance zones occupy a large portion or cover the field of vision completely. The assumptions necessary for a successful application of the phase-contrast method can be formulated correctly by the condition that the amplitude of the center of gravity vector of the amplitude-phase-vector diagram of the object field must remain of the same order of magnitude as the amplitude of the light passing through the object field. (The amplitude-phase-vector diagram will be discussed later.) The aim of the investigations described here was to eliminate these restraining conditions, so that the method could be applied to any field and to replace the tedious photometric brightness measurement in the image field by a band field with easily evaluable black-white effects. The possibility of superposition of any wedge fields in the course of this development entails no loss of sensitivity.

In the further course of this treatment, it is attempted to explain the principle and the details of the method as simply as possible but in enough detail for understanding and correct application. The experimental data by Gayhart and Prescott (ref. 6) obtained with a schlieren apparatus using a very narrow light slit are also explained.

At this point I want to mention duly the eager cooperation of Mr. A. W. Meijer who helped indefatigably with the preparation (frequently requiring much patience) and performance of the tests, the evaluations and the providing of illustrations for this report.

2. PHYSICAL TREATMENT OF THE THEORY OF THE METHOD

(a) Image Forms of Simple Optical Systems

The explanation of the interferometric phenomena in question is, naturally, based upon the wave theory of light.

Proceeding from the well-known Frauenhofer diffraction phenomena from a slit, which is illuminated by vertically incident, parallel light, the light is propagated in all directions perpendicular to the slit according to Huygen's principle. Now, angles α_z can be identified (fig. 1) for which, by reason of their different wave length, a second beam can be found for each light beam which shows a phase difference of a half wave length $\lambda/2$ to it. When these beams are coincident in the focal point of a lens, they extinguish each other. On a screen S, the image then appears with a brightness distribution such as represented qualitatively by figure 2.

The beam directions for the extinction of the light can be described, according to figure 1, by the relation

$$\sin \alpha_z = z \frac{\lambda}{l} \quad \text{with} \quad z = 1, 2, 3 \ldots \tag{1}$$

with l = width of slit.

Along the incident light, that is, $z = 0$, the brightness is maximum. The point of extinction on the screen referred to the point of symmetry, is expressed by the equation

$$d_z = R \tan \alpha_z \tag{2}$$

where R denotes the distance of the screen from the lens, in this case, the focal length. Limited to small angles α_z as is generally permissible, in case l is not extremely small, since the refractions of higher order can be disregarded,

$$d_z = z \frac{\lambda R}{l}$$

by reason of

$$\tan \alpha_z \approx \sin \alpha_z$$

The total width of the central intensity maximum from zero passage to zero passage for the slit is then

$$D_s = 2d_1 = 2 \frac{\lambda R}{l} \tag{3}$$

Considering the same phenomenon but with a circular diaphragm of radius γ instead of the slit, the picture on the screen shows then a similar but coaxial intensity distribution. The central intensity maximum, frequently termed diffraction disk, follows then as

$$D = 2.4 \frac{\lambda R}{2\gamma} = 1.2 \frac{\lambda R}{\gamma} \tag{3a}$$

Thus the parallel light mentioned at the beginning can be visualized as originating from a point source of light in the focal point of the lens and the described diffraction pattern on the screen is then the image of this light source. From the relation (3a), it is seen further that this image shrinks more and more coaxially in proportion as the lateral dimensions of the transmitted parallel beam, that is,

the diaphragm radius, increases. Theoretically, it is not even necessary that a real diaphragm is presented. The final dimension of the image forming lens can already be regarded as such. A clear point reflection of the light source would be obtained only when the diameter of the diaphragm or the lens increases beyond all measures.

Continuing a step farther and replacing the screen by a lens set up behind so as form a picture of the diaphragm in a new plane (fig. 3), a sharp picture of it is obtained when a sufficient number of diffraction maximums can enter in this lens. But if the aperture of the lens is continuously narrowed, the haziness of the diaphragm picture increases. When only the central intensity maximum is able to pass through, the result is a washed out spot of light of approximately the size of the original diaphragm picture with outwardly continuously decreasing brightness. If the aperture is restricted to a point, the result is, according to Huygens' principle, that instead of the diaphragm picture the entire image plane is lighted up to infinity with brightness decreasing monotonously from the center.

For a thorough understanding of the subsequently described method, these phenomena and the consequences connected with it are of such decisive importance that it is deemed appropriate to discuss the last described mental experiment again in reversed order.

If, from the diffraction image of the light source in the focal plane, only a very small quasi-pointlike sector of the center is admitted for image forming, it results in an infinitely great lighted area instead of a diaphragm image. When this sector is enlarged a little in every direction, the additional light increases the central brightness of the image and interferes with the border zones, so that the brightness in the central image is more evenly increased and the brightness decrease in the border zones becomes more spontaneous. With it, the central field becomes more and more defined and stands out more. Now if the entire diffraction image of 0 and 1st order are admitted for image forming, the diaphragm image already begins to become sharply delineated until the picture becomes more and more perfect as further diffraction orders are admitted.

If the same experiment is made with a variable slit instead of a circular lens aperture of variable diameter, the result is an identical blurring process in the image plane but limited to the direction perpendicular to this slit. The form of the light source and the shape of the diaphragm representing the object field play no part in theory.

The same statement made for the diaphragm in parallel light relative to the diffraction image of the light source in the focal point of an inserted lens and the image of the diaphragm with the aid of a second lens applies to the arrangement according to the coincidence method, that

is, a light source in the vicinity of the center of curvature of a spherical mirror. (See fig. 4.) Its reflection is also the same diffraction figure symmetrical to the position of the light source in the vicinity of the curvature center. If the mirror forms only a small spherical sector, the same relation

$$D = 1.2 \frac{\lambda R}{\gamma} \quad \text{or} \quad D_s = 2 \frac{\lambda R}{l}$$

applies again, where R is the curvature radius and γ the radius of the mirror, and l the width of a slit placed on the mirror.

The theoretical equality of both phenomena follows from the fact that, in both cases in the critical section, that is, the diaphragm in one case, the spherical mirror on the other, the light shows equal phase.

The kernel of the discussion is briefly as follows:

In the discussed optical system, any diaphragm, even where the finite dimensions of the employed lenses or mirrors can action as such, forms a diffraction figure of the light source. Furthermore, the diffraction orders used for illustrating the plane of the mirror, lens, or diaphragm define the type and quality of this image. Lastly, it is emphasized again that the diffraction center, that is, the diffraction of 0 order, considered as independent light source, covers the entire image of the object plane comparatively evenly and even beyond on the surrounding field, although with considerably less brightness.

(b) The Object Field in Vector Representation and Its Interferometric Representation

By way of illustration, the simple optical arrangement of the coincidence method shown schematically in figure 4 is to serve as basis; all the phenomena described with it occur in completely similar manner when parallel light is used, so that a separate representation of the two cases is superfluous. The individual addition of a diaphragm is also omitted, but the border of the mirror, or its total diameter for the parallel beam, is considered as characteristic diaphragm quantity l and an arbitrary plane in the parallel beam, respectively; the mirror plane or the plane extended immediately in front, in the coincidence representation, is designated as object plane.

Supposing that on a mirror to be regarded as ideal, several transparent models as indicated in figure 5(a) are present which exert an

influence on the phase of the light but not the amplitude. These models on the mirror surface are numbered and the assumedly corresponding light vectors are represented in an equally numbered vector diagram. (See fig. 5(b).) The vector length indicates the amplitude, its direction, the phase. Owing to the assumed transparency of the models, the end points of all these vectors lie on a circle around point 0. These light vectors can be visualized as being split in two components, one to consist of a unit vector for all of which it is assumed that it represents a portion of the light covering the entire mirror surface evenly. According to Zernike (ref. 1), there is such a one which is found by forming the center of gravity of the vector diagram (fig. 5(b)), after adding the lighted up area to each end point of the plotted vectors. This center of gravity is represented by A in figure 5(b).

The light represented by the vector OA forms then as image of the light source a diffraction picture as described earlier, with a central intensity maximum of

$$D = \nu \frac{\lambda R}{l} \quad \text{with} \quad 2.0 < \nu < 2.4 \tag{3b}$$

depending on type and shape of the object field. In this central intensity maximum, the total light represented by the vector length OA can be visualized concentrated, in first approximation. This plainly follows from the intensity distribution of the diffraction picture of the light source (fig. 2(b)) wherein the higher orders of diffraction are negligible within the scope of a first approximation relative to the 0 order.

Letting this diffraction center experience a special fate by which it becomes distinguished from all others, the assumptions for the desired interferometric effects can be produced. This can be effectuated in various ways. The "dark-field effect" long used in microscopies can be created by completely covering the diffraction center, or the "phase-contrast effect" can be produced by adding a phase disk as suggested by Zernike, which varies the phase of the central light abruptly and, if necessary, reduces the amplitude too, or the entire remaining field can be made strongly absorbent while leaving only the diffraction center unaffected. This is termed "field absorption."

According to the foregoing, the light emitted from the diffraction center is comparatively evenly distributed over the entire area of the image to be formed by the mirror. Thus, after taking one of the cited steps, the central light interferes like a veil over the image field. Without partial interference of the diffraction picture of the light source, an image of the object plane true in amplitude and phase would result. The eye would see no differences in this case because the amplitude was assumed identical in every point and does not respond to

phase differences. But with special treatment of the central diffraction image, it results in a picture which can be best explained on the basis of the vector diagram. (See fig. 5(b).) By plotting, as example, three vectors (1, 3, and 4) with and without interference in the diffraction image, the results shown in figure 6 are obtained. The original vector is shown as chain dotted line, that as seen by eye as solid line. The following is manifest:

(1) The dark-field method is equivalent to a shrinkage of the center of gravity vector OA to length zero and thus to a shift of the original zero point O to the new zero point O_D at A.

(2) The addition of a phase disk corresponds to a rotation of the OA vector about A, that is, about the angle by which this changes the phase. Thus, figure 5(b) shows the new zero points O_P', O_P'', and O_P corresponding to phase rotations through $\psi = 90^\circ$, 180°, and 270° or, respectively, -90°.

(3) The writer's proposal (field absorption) is equivalent to a relative increase of the vector OA, hence to an effective displacement of the zero point leftward by an amount that is defined by the measure of the intended absorption. If the absorption of the material surrounding the diffraction center indicates a permeability of 1/2, 1/3, or 1/4 of the amplitude, the new effective zero points O_{E2}, O_{E3}, or O_{E4}, shown in figure 5(b) are produced. This corresponds to absorptions referred to intensity, hence, the square of the amplitude in the same sequence of 75 percent, 88.9 percent, or 93.7 percent.

As a result, the different vectors show different lengths in the image of the object plane and are visible to the eye as differences in brightness. By way of contrast, the object plane perhaps manifests opaque objects (such as a model in the flow, for example) whose image would coincide with point O in the vector diagram, no longer as dark but with a brightness corresponding to the distance OO_X, where O_X indicates the newly created zero point depending upon the chosen method.

It should be clear from the aforegoing that the light concentrated in the diffraction center can actually be regarded as a component of the local light vectors common to the entire image of the object field. However, this component is not an arbitrary one of the infinite number of imaginable components; it must be the center-of-gravity vector OA correlated to the particular vector diagram, as is readily proved by a simple approximate energy consideration. The phase-contrast method is particularly suitable for this demonstration, inasmuch as none of the light is suppressed by absorption, hence that according to the energy principle it can and must be postulated that the sum of all the light in the image

of the object field must remain the same independent of the affected manipulations.

At the personal suggestion of Mr. Greidanus of the N.Y.I. Laboratory, this demonstration is described in the following form:

Supposing the vectors of the zones 1, 2, 3 . . . are expressed by

$$e_n = \cos \varphi_n + i \sin \varphi_n \quad \text{with} \quad n = 1, 2, 3 \ldots$$

and $|e_n| = 1$; the component OA common to all vectors assumed concentrated in the diffraction center to be

$$p = p \cos(\varphi_0 + i \sin \varphi_0)$$

Then the individual vectors follow as sum of the two components

$$e_n = b_n + p$$

$$e_n = \left[(\cos \varphi_n - p \cos \varphi_0) + i(\sin \varphi_n - p \sin \varphi_0)\right] +$$

$$\left[p \cos \varphi_0 + ip \sin \varphi_0\right]$$

Next, on the basis of experimental experience, it is assumed that an interference in the diffraction center has practically no effect on the first component b_n, but merely on the second component p imagined as being concentrated there. When the latter is rotated through angle ψ in the phase, p becomes

$$\overline{p} = \left[\cos(\varphi_0 + \psi) + i \sin(\varphi_0 + \psi)\right] p$$

and after reuniting the components in the image of the object field, e becomes

$$\overline{e}_n = b_n + \overline{p}$$

$$\overline{e}_n = \cos \varphi_n - p \cos \varphi_0 + p \cos(\varphi_0 + \psi) + i\left[\sin \varphi_0 - \right.$$

$$\left. p \sin \varphi_0 + p \sin(\varphi_0 + \psi)\right]$$

From this, it can be easily computed that the local image intensity becomes

$$|\bar{e}_n|^2 = 1 + 2p^2(1 - \cos\psi) - 2p\cos(\varphi_n - \varphi_0)(1 - \cos\psi) + 2p\sin(\varphi_n - \varphi_n)\sin\psi$$

Now the initially formulated energy relation can be written in the form

$$\sum |\bar{e}_n|^2 F_n = \sum |e_n|^2 F_n \quad \text{or} \quad \sum |\bar{e}_n|^2 F_n - \sum |e_n|^2 F_n = 0$$

with the premise that this condition is fulfilled independent of the effected phase rotation ψ. The factor F_n indicates the areas or zones of the object image related to the corresponding light vectors in which they occur. Insertion of the above squared expression, while allowing for the fact that $|e_n|^2 = 1$, gives

$$2p^2(1 - \cos\psi)\sum F_n - 2p(1 - \cos\psi)\sum \cos(\varphi_n - \varphi_0)F_n + 2p\sin\psi\sum \sin(\varphi_n - \varphi_0)F_n = 0$$

The stipulated independence of ψ is then fulfilled only by the conditions

$$\sum \cos(\varphi_n - \varphi_0)F_n = p\sum F_n$$

and

$$\sum \sin(\varphi_n - \varphi_0)F_n = 0$$

which, as is seen, represent directions for φ_0 and p which define the vector $OA = p$ as center-of-gravity vector.

This consideration is rigorously valid theoretically. Its approximately close but not rigorous proof by experiment rests, in this case,

not on the inadequacy of the theoretical treatment but on the experimental impossibility of realizing a factually rigorous separation of components, since fundamentally both cover the entire plane of the diffaction image. The b_n components can be considered as spread so generally over the entire field that the portion coincident with the diffraction center of the evenly lighted-up mirror is practically of no significance. But the center-of-gravity vector in the diffraction center shows a concentration high enough to realize the desired effect with sufficient approximation.

The fact that, by phase rotation or some other interference of this center, the higher diffraction orders of the center-of-gravity vector cannot be included has an effective not completely uniform decrease of the average brightness of the object field as a result and as compensation the radiation of the remaining light over the image borders.

The quantitative reliability of the interference pattern obtained with it does not suffer, at least as long as the magnitude of the affected area remains within the dictates imposed by equation (3b).

(c) Discussion of Possible Interference Formations

From the foregoing, it is seen that the resultant center-of-gravity vector OA is, after its special treatment, the carrier of the interferometric effects.

Beginning with the phase-contrast method, the exact conditions can be easily illustrated on the basis of figure 7, where the locus of all possible end points $O_{Pr}A_r$, that is, after -90° phase rotation, is plotted. The result is a straight line starting at an angle of 45° with respect to the original vector OA from the original zero point O. The subscripts γ at the points O_{Pr} and A_r indicate corresponding vectors, whereby γ indicates the amount of the vector referred to the radius 1 of the principal vector diagram. Bearing in mind that the occasional points O_{Pr} then denote the new zero points to which all light points of the object field in the illustration are to be referred, it is apparent that at first the contrasts to be achieved increase with increasing γ, but only up to $\gamma \approx 0.7$, where $O_{P0.7}$ then lies on the circle, hence contrasts of double brightness up to absolute black can appear.

A further increase of γ shifts the new zero point beyond the circle, so that greater brightness but no complete extinction is possible. The proportion of extreme brightness can then no longer become zero or infinite, but must remain finite. To prevent this, Zernike

(ref. 1) suggested to cover the phase disk with a more or less strongly absorbing layer. This reduces the slope of the O_{Pr} straight (dashed), so that, if appropriately covered, the new zero point falls on the circle again and hence renders extreme effects possible. A total absorption returns the zero points O_{Pr} to the relative points A_r and yields the known dark-field effect, which thus proves to be only a special case of the phase-contrast method.

After these deliberations, it is clear that a really well evaluable contrast-rich image is obtainable only when the length of the center-of-gravity vector is no less than about $\gamma = 0.4$. But this means that only objects with relatively small phase variations in the object field must be involved, or that in the presence of greater irregularities they are limited to a small area compared to the total field. This might be the main reason why this method has not been applied to flow investigations, which usually deal with very severe disturbances frequently spreading over the entire field.

The difficulties encountered by the dark-field and phase-contrast method for a too small vector OA, can, however, be avoided by the suggested absorption of the field surrounding the center of diffraction, since it, as already stated, is equivalent to an arbitrary relative vector increase, depending upon the degree of chosen absorption. Thus satisfactory bright-dark effects can be obtained also with transmission of the vector diagram, if the center-of-gravity vector OA is very small. The extent of the absorption must be so chosen that the new zero point O_P falls about on the external beam of the vector diagram. In practice, up to now a field absorption of about 95 percent has generally proved very favorable. This method fails theoretically only in the practically nonexisting cases of zero vector OA.

The discussed interferences of the diffraction center are effectuated by some auxiliary means such as cover plate, phase disk, or free passage in the absorbent field. All these auxiliary means are hereafter gathered under the collective terms as interference plate, interference slit, or interference circle, depending upon shape.

Thus far, only the interference of the central diffraction image of a quasi-point source of light was in question and the application of interference disks associated with it. But in theory, an interference slit spanning the entire aperture of the lens can also be used instead. The result is, as briefly stated before, that the central light is then dispersed only perpendicular to the slit and distributed over the object field rather than toward all sides. Admittedly it is true, even though with limitations discussed in section (3b) what was stated in the foregoing regarding the vector diagram and its center-of-gravity vector, but in a somewhat different form. In this case, a vector diagram and

a center-of-gravity vector is no longer representative for the whole object field; fundamentally there exist an infinite number of such for every object field, each of which is characteristic for one section of the object field. The consequence is, that fundamentally, aside from exceptional cases, one assumption is no longer sufficient for a complete, quantitative determination of the object field, but two with mutually shifted interference slits are necessary.

Compared to the interference disk, the use of an interference slit has four direct practical advantages:

(1) The extent of the light source which in principle must be smaller than the diffraction center of its figure is limited in one direction only. So, instead of a quasi-point source of light, a slit-like source of light can be used and much more light made available.

(2) In fact, it requires just such treatment to make superposition of wedge-shaped fields possible, which proves very desirable in many cases for increasing the measuring accuracy.

(3) Excellent light-dark effects are attainable scarcely inferior to those of a normal interferometer.

(4) In object fields with two wedge fields of different directions superposed, as is frequently the case in open jet supersonic wind tunnels with glass walls, which manifest wedge errors, these wedge errors can be eliminated and satisfactory test data obtained.

These are the advantages which give in the majority of cases the use of the interference slit the preference.

Lastly, there is yet a third possibility which embodies advantage (1) cited above and the advantage accruing from the use of the interference disk, namely, of obtaining a quantitatively completely determinable result with a single photograph. (For the sake of completeness, it should be stated that, in general, just as with every normal interferometer, one or two schlieren photographs are required in order to determine whether a sequence of lines about density increase or decrease are involved.) This third possibility is the use of a circular source of light with a corresponding interference circle. The light-dark effects obtainable with it are, however, not good save in exceptional cases, and wholly inadequate in many instances. This rules out the superposition of a wedge field.

The conditions are exemplified on two examples, with exception of the superposition of wedge fields to be discussed later, by the interference figures (figs. 8 and 9). For comparison, the photographs obtained with a Michelson interferometer in the Zeeman laboratory at

Amsterdam have been included. Since the image field there was considerably smaller than the objects, the field had to be made up from a series of partial photographs. The possibilities of displacement of the model were so primitive that a slight misalinement was unavoidable. It explains the poor fitting of one sector to the next on the interference band.

The evaluation of the figures obtained with interference slit are discussed in detail in section (4). As to the photographs in figures 8 and 9, it may be stated that in fact the combination of two photographs made with mutually shifted interference slit affords a picture on a par with the Michelson interferometer photographs. (Compare section 5, fig. 24.)

3. REPRESENTATION OF LIGHT SOURCE AND IMAGE FORMATION ON SOME SPECIAL OBJECT FIELDS

(a) Wedge-Shaped Density Variation

A rectangular object field is assumed which in depth, that is, in direction of the transmitted light, is bordered by two parallel glass plates of distance t. The object field is of width l; air exists between the glass plates, the density of which shows a constant increase grad $\rho = \rho' =$ constant in the direction in which l is measured. The light passes through uneven optical wave lengths in various sections perpendicular to this gradient. As a consequence, the light in gradient direction is no longer in phase. This signifies on the one hand, considered from the point of view of the method treated here, that the light vector rotates uniformly in the vector diagram of the object plane. On the other hand, by reason of the fundamental relationship between a prism and the field discussed here (termed wedge field hereafter), it results in a deflection of the light. In order to be able to judge the consequences associated with it exact, a quantitative examination is indicated.

The refractive index for air is given by the relation (ref. 7)

$$n = 1 + a\rho$$

with the density ρ and a constant a dependent on the wave length of the employed light. Its value is computed too from the relation

$$(\bar{n} - 1)10^6 = 272.643 + 1.2288\lambda^{-2} + 0.03555\lambda^{-4}$$

where λ = wave length of light expressed in μ, and $\bar{n}$ the index of refraction at standard atmosphere, hence, at a temperature of 15° C and a pressure of 760 mm Hg.

For the two principal lines of the mercury spectrum, it is

$$\lambda_1 = 0.546\mu \text{ (green line)}, \quad a_1 = 0.002226$$

$$\lambda_2 = 0.365\mu \text{ (ultraviolet line)}, \quad a_2 = 0.002280$$

Introducing the length coordinate x in direction of the density gradient and shifting its zero point in the center of the object field where the density ρ_m prevails, the variation of the refractive index follows as

$$n = 1 + a(\rho_m + \rho' x) \tag{4}$$

and the optical path length within the object field of depth t as

$$s = nt = t\left[1 + a(\rho_m + \rho' x)\right] \tag{5}$$

The total optical path difference made nondimensional by the wave length of the employed light is equal to the total phase difference $Z = \Delta\varphi/2\pi$ and follows as

$$\frac{\Delta s}{\lambda} = \frac{ta\rho' l}{\lambda} = \frac{\Delta\varphi}{2\pi} = Z \tag{6}$$

l = width of object field.

The center-of-gravity vector of the vector diagram of the object field follows, with stipulation of $\varphi = 0$ for $x = 0$, as

$$|OA| = \frac{2}{l}\int_{x=0}^{l/2} \cos\varphi \, dx \tag{7}$$

since, on account of the symmetry to the abscissa $\varphi = 0$, the components perpendicular to it cancel out. This transforms with the phase relation (6) in general form

$$\varphi = 2\pi \frac{ta\rho'}{\lambda} x$$

into

$$|OA| = \frac{2}{l}\int_0^{l/2} \cos\left(2\pi \frac{ta\rho'}{\lambda} x\right)dx = \frac{\lambda}{\pi ta\rho' l} \sin \frac{\pi ta\rho' l}{\lambda}$$

Thus, the center-of-gravity vector is given as

$$|OA| = \frac{\sin \pi Z}{\pi Z}$$

in relation to $Z = \Delta\varphi/2\pi$ and plotted in figure 10(a). The center-of-gravity vector is zero for all integral $Z = 1, 2, 3 \ldots$, which is readily apparent because it signifies that the vector diagram is exactly Z-times run through, hence, is in equilibrium in the zero point.

Such a state forms one of the very rare situations occurring in practice in which the method in question is unable to form interferences. In all other cases, the resulting vectors OA whose length, that is, the brightness representing it, are considerably affected by Z and, in general, tendency to such an extent that the momentary maximums of the individual intervals decrease substantially with increasing Z. Hence, it is possible to secure interference figures, but with the dark-field and phase-contrast method only when Z is restricted to small values, but unlimited with field absorption.

Comparison of figure 2(a) with figure 10(a) indicates that both figures are strikingly similar; moreover, bearing in mind that relation (6) through

$$ta\rho' = \alpha \tag{8}$$

becomes equation (1)

$$\alpha = Z \frac{\lambda}{l}$$

for small angles α, the suspicion suggests itself that, fundamentally, the phenomena are alike in the sense that identical diffraction figures of the light source occur in both cases, whereby that of the last described test relative to the diffraction at the slit is laterally displaced as a result of the diffraction by the wedge field. The supposition is extremely plausible and signifies that, in consequence of the displacement due to the wedge field in place of the diffraction center a

higher diffraction order is represented on the geometrical axis of symmetry of the optical system. This assumption is confirmed by the subsequently adduced proof that the relation defined in equation (8) actually exists as a result of the diffraction of light by the wedge field.

This proof is based on equation (4) which in conjunction with the relationship between index of refraction and the ratio of local velocity of light c to that in vacuum c_0

$$n = \frac{c_0}{c}$$

gives for the former

$$c = \frac{c_0}{1 + a\left(\rho_m + \rho' x\right)}$$

which, since $a\left(\rho_m + \rho' x\right) \ll 1$ for air can be written in the form

$$c = c_0\left[1 - a\left(\rho_m + \rho' x\right)\right]$$

Thus the wave front rotates about point x_0 in which c would be $c = 0$. This results in the conjunction

$$x_0 = \frac{1 - a\rho_m}{a\rho'}$$

and, by reason of $a\rho_m \ll 1$

$$x_0 = \frac{1}{a\rho'}$$

The light, which as is known is propagated perpendicular to this wave front, is rotated therefore by the same amount as it. As the density field that produces this rotation is to have the depth t, the light itself is deflected in its entirety through the angle

$$\alpha = \frac{t}{x_0} = ta\rho'$$

The agreement of this result with the definition (8) furnishes the desired proof, namely, the suspected quasi-identity of the two apparently different cases involved.

A density gradient produces, accordingly, a displacement of the optical zero point of the diffraction figure relative to the geometrical zero point of the placement in the plane of the light-source figure, without entailing any subsequent variations. This result furthers the expectation that it should be possible to produce a band field in the plane of the object image by a specific displacement of the interference slit from the geometrical zero point of the system perpendicular to the slit, even in a field without gradient, and thus create the impression of the existence of a wedge field in the plane of the object. That this expectation proves correct is borne out by the photographs in figure 11, obtained for a field without any gradient by a continuous shift of the interference slit from the zero position.

The quantitative relationship between this simulated gradient and displacement ϵ follows as

$$\epsilon = \alpha R = ta\rho' R \quad \text{or} \quad \rho' = \frac{\epsilon}{taR} \tag{9}$$

as is readily apparent from figures 1 and 4.

Obviously, the reversed process of the gradient of an existing wedge field can equally be determined the same way by measuring its displacement ϵ with respect to the geometrical zero point, which is necessary to let the object field appear as free from gradient. With that, an arbitrary but known wedge field can be superimposed on each object field by a corresponding displacement of the interference slit. This is the second extremely decisive extension of the possibilities of this method.

But if it is desired to get rid of the length measurement ϵ, which is rather inconvenient in practice, the gradient to be determined, whether actually present or artificially superposed, can also be defined interferometrically. This is accomplished by measuring those interference bands per length h in the object field in direction of the displacement, that is, perpendicularly to the interference slit

(1) which are produced by creation of a wedge field on the object without gradient,

(2) those which became additive or diminished at superposition of the wedge field on an arbitrary object field, or which remain after removal of the latter, such as in flow measurements with still air before or after each test,

(3) those that originate after removal of the object, in the case where compensation of an existent wedge field took place by displacement,

(4) those arising in an auxiliary field without gradient which has been fitted at an appropriate point, as for example, obtained by hollowing out the model in direction of the light passage, in flow measurements.

The gradient follows by equation (6) with h instead of l as

$$\rho' = \frac{Z\lambda}{\tan h} \tag{10}$$

In order to be able to determine the prefix of the gradient, the direction of the displacement must be considered, while bearing in mind that the light is always refracted in direction of the rising gradient. In other words, the gradient is positive in the direction in which a displacement of the interference slit is accompanied by a reduction of the number of bands per length.

At this point, a question arises that may intrude itself upon many readers, namely, how the artificial production and the superposition of ostensible wedge fields could be reconciled with the concept of the vector diagram of the object plane discussed in section 2(b) and its interference by modification of the center of gravity. The energy considerations at the end of section 2(b) had proved that, if interference phenomena are to be produced in the described manner, it can be accomplished only by way of the center-of-gravity vector of the vector diagram. But this is, as stated, reflected in the diffraction center of the uniformly lighted mirror. How can this concept be reconciled with the production of ostensible wedge fields which precisly calls for a migration from this center of diffraction?

The aforementioned energy consideration had proved that the existence of a phase-contrast effect was contingent upon the coaction and the interference of the center-of-gravity vector of the related vector diagram. On the other hand, the experiment has proved that such an effect could be secured not only with an interference disk or slit in the focal point of the system but also outside of it, even with pure phase rotation. In these cases, the use of field absorption had usually proved more favorable for obtaining better contrasts, owing to the then usually small vector, although in principle a pure phase rotation also yields interference figures. From the comparison of these two facts, the general conclusion can be drawn that the light in each space point can be regarded as center-of-gravity vector of all vector diagrams that

can be constructed on spherical shells around this point, or on cylindrical shells, by the use of an interference slit, that is, in an included angle perpendicular to the interference disk or slit, defined by the relation (3b) in the form

$$\vartheta = \frac{l}{R} = \nu \frac{\lambda}{D} \quad \text{with} \quad 2.0 < \nu < 2.4$$

where D denotes diameter or width of interference disk or slit. In practice, it means that a displacement of the interference slit is automatically followed by a change in the correlated vector diagram in such a way that a lateral displacement in the plane of the original diffraction figure causes the effective object field to rotate correspondingly, which in first approximation is equal to a wedge field and in case of displacement toward the object field or away from it is equal to a reduction or increase of the effective curvature radius R of the object field, hence to a more or less concave development of it. (See fig. 10(b).) The last phenomenon can be of great practical significance insofar as it provides the possibility of compensating eventual concave or convex errors of the glass plates closing off the object field by a simple displacement of the interference disk or slit perpendicular to the plane of the diffraction figure, just as wedge errors can be eliminated by a lateral displacement in this plane. Moreover, there is no change involved, in these cases, in the discussed mode of consideration of the vector diagram and the possibility of its interference for obtaining interference figures of the correlated object plane.

(b) Edge Effect and Band Formation

The aforementioned possibility of band production by displacement of the interference slit from the zero position is easily proved experimentally in its simplest form. Figure 11 shows such a photoseries in which the object field is formed from a carton by a rectangular sector. By successive shifting of the vertical interference slit in horizontal direction, one, two, and more vertical bands are produced.

If the light and interference slit were replaced by a point source of light and an interference disk, the position relationship between diffraction of zero order and interference disk would always be unequivocally defined. In consequence, a certain shift from the zero position would always reveal bands of identical width and direction, independent of the form of enclosure of the object field.

But, if an interference slit is used, the unequivocal position relationship is lost. It is then no longer a second quasi-point source of light that produces the interferences, but an unevenly covered slit

of light whose individual points exhibit variable coordinates relative to the center of diffraction. The fact whether the original light source itself is a point or parallel to the interference slit is of no significance since, of course, only coherent lights can interfere with one another.

Because the distribution of light of the diffraction pattern is markedly dependent on the form of the enclosure as well as on the density variation in the object field, it also applies to the light distribution that falls on the interference slit. Hence it is to be expected that the ensuing interference figures themselves are affected by the form of the borders of the object field. This is confirmed by figure 12 which was obtained by interference slit displacement on a circular object field, and yet shows no vertical straight interference bands.

For a better understanding of this phenomenon, two examples are discussed, although limited to the rough effects of first approximation, since an exact treatment would in all probability be rather extensive and does not appear to be absolutely necessary at the present state of development. To define the concept, it is assumed that the interference slit is fitted vertically and shifted horizontally.

The first example is illustrated on a "Swiss Cross" (fig. 13) made as vector from cardboard and in which various ostensive wedge fields are to be produced by displacement of the interference slit. For this, two superposed diffraction figures are obtained. One results from the comparatively long central crossbeam A and forms the diffraction maximums of distance δ of the higher orders indicated as black dots in figure 14. The two short projecting arms B, only 1/3 as wide as the longitudinal, form diffraction maximums at distance 3δ of the higher orders, indicated by squares in figure 14. It follows that, at displacement of the slit from its zero setting, first one, then two bands are produced in the long transverse beam, while the short beam section reveals nothing yet. Much better than figure 14 for a quantitative definition is the brightness distribution of the two superposed diffraction figures reproduced in figure 15, which shows the various slit settings corresponding to the various photographs (fig. 16) of the "Swiss Cross." With the aid of this representation, all photographic phenomena can be explained practically without comment, even such minor details as that at zero slit setting the borders of the A-zone are illuminated much brighter than those of the B-zones (fig. 16(a)). This is due to the fact that, through the slit in the A-diagram, much more light overlaps than in the B-diagram (fig. 15). Furthermore, the bands in the B-fields of figures 16(e) and (h) indicate better contrasts than those visible in figures 16(d), (f), and (g). The reason for this is also directly apparent from figure 15. It is seen that, in the cases conforming to figures 16(d), (f), and (g), the slit with sector coincides

with the B-brightness distribution, where this increases or decreases and hence relatively less light is available for interference formation than in those of figures 16(e) and (h), where sectors from brightness maximums are presented.

It is of interest to note that this example reveals, for the first time, the surprisingly visible, separistic behavior of different horizontal zones, in this case, the boundary lines between A and B, whose existence with the use of an interference band had already been repeatedly asserted in the foregoing.

The example indicates, further, very plainly that the first band is not produced at a distance equal to an optical path difference of 0.5λ from the zone boundary as a superficial inspection might indicate, but at a distance that may vary between 0.5λ and 1.0λ, conformably to the two passages of the diffraction figures of first order through zero, shown in figure 15. This is the sole remaining and unavoidable inaccuracy inherent to the interferometric principle in general, not so much to this special method alone. By the phase-contrast method, this range would, as consequence of the phase rotation, be about 0.125λ to 0.625λ but with, usually, very much weaker contrasts for the previously cited reasons. An illustrative example for it is given in figure 17, which, of course, shows no rigorously symmetrical figure.

However, this uncertainty in the boundary zones detracts nothing from the fact that on more than one existing band their mutual distance exactly corresponds to an optical path difference of one wave length.

The second example is illustrated by means of a square set on its tip (rhombus) so that the edges slope at $\pm 45^{\circ}$ with respect to the interference slit. Following the experimental proof of the separistic behavior of the various zones perpendicular to the slit in the first example, it is attempted to derive the interference figures to be expected for displacement of the slit from the zero position and to illustrate it in figure 18.

For a clear outline of the situation involved, figure 18(a) shows the normal figure of the lines of equal density for the particular field. The solid lines indicate blackening, the dashed lines the regions of maximum brightness. In principle, it is immaterial whether a real or fictitious wedge field is involved, such as can be obtained with an interference disk shifted from its zero position or with a Mach-Zehnder interferometer by tilting one of the mirrors with respect to the other. Now the question is what kind of an interference figure would occur with an interference slit under the same conditions?

In order to make the discussion clearer and facilitate mutual reference, the fields of figure 18(b) and (c) are divided into zones by

dotted horizontal lines in such a way that these dotted lines indicate exactly, at the same time, whole multiples of a wave length as optical path differences. Along these lines, no interference formation is likely to be possible for a wedge field, when it actually starts along this linear from the center-of-gravity vector of the vector diagram (fig. 5(b)), since it is zero at that point.

Holding to this concept of interference formation for the time being, the following relationship prevails:

If the total optical path difference from one border to another is less than one wave length, the new zero point O_E would lie in the vector diagram (fig. 5(b)) for this zone at the left of the original zero point O, that is, the center-of-gravity vector OA and with it O_EA is in phase also with the vector of the zone center. However, if the total path difference is more than one but less than two wave lengths, O_E lies to the right of O, that is, OA is in opposite phase to the zone center. At a difference of more than two, O_E lies left again, at more than three, to the right, etc. So, if this concept of the cause of interference through an unequivocally defined center-of-gravity vector proves true, it means that in the first instance the zone center should show maximum brightness, in the second, maximum darkness, then bright again, etc. (See fig. 18(b).) The result would be dark line elements whose contrasts would be greatest in the center and decrease toward the outside and become zero upon reaching the first-following dotted line, since OA itself becomes zero. The anticipated contrast yield is accordingly indicated by the local thickness of blackening.

An identical interference figure but with unchangeable contrasts in the individual blackening elements, would result if the object had the step contour shown in figure 18(c) instead of the rhombus form. After the results with the "Swiss Cross," it can be stated that in this case the represented figure would be actually obtained. However, it is to be assumed that this figure does not appear at once on the rhombus field, because the direction of diffraction is, as known, perpendicular to the wave front, hence perpendicular to its edges on the bounded field. If these are parallel, the principal direction of diffraction and with it the intersecting of it with the interference slit is unequivocally defined, and it is this point that produces the interference figure occurring as independent source of light. On the other hand, if the two lateral zone borders are not parallel, two principal directions of diffraction perpendicular to these borders result, besides that of the zone flanks directed parallel to the interference slit, hence, two intersection points with the interference slit. Thus these two independent radiating light sources cause two independent band systems parallel to the field fringes. The center-of-gravity vector concept is therefore ruled out and its validity is thus restricted to very special cases.

In order to arrive at a quantitative conception, the situation may perhaps be imagined to be such that the rhombus field is obtained from a superposition of the step contour with a number of small, positive and negative triangles of light bounded by the dotted line and the contour in figure 18(c). What is meant by this is that these triangles of light represent additional light sources, whose phase structure represents the continuation of the rectangular field in the positive case, and as being in opposite phase with it in the negative case. Accordingly, step contour and rhombus form merely do not differ at the half zone heights. There the superposed light sources are zero, so that it is assumed that the same interferences occur there also in both cases and that the existing blackening on the rhombus represents the intersection points of the two fringe systems. The final result to be expected on the rhombus is the interference figure of figure 18(d), which in many respects is confirmed by the experiment (fig. 19(a)). The latter shows, in fact, band systems shifted parallel to the edges toward the inside (compare figs. 12 and 20), but, contrary to the expectation cherished according to the previous speculation, does not seem to spread over the entire field. This divergence may be due to two causes. Either the interference slit was not small enough for the total field width so that the light was not uniformly enough distributed from both sides over the field, or else it is the result of the likewise partial light of diffraction falling on the interference slit, which, starting from the corners of the rhombus is distributed in all directions within $\pm 45^{\circ}$. Even the photographs on the small rhombus (fig. 19(b)) fail to give definite particulars, for there too the same effect is noted on few bands. Only the last figures with many bands create the impression of complete agreement with the theoretical network of figure 18(d).

The appearance of two continuous systems had proved that the assertion voiced in section 2(c) actually does not prove correct in general. According to that statement, the interference phenomena with interference disks or slits differed only in the interference being due to a resultant vector for the whole field in the first case, and the center-of-gravity vector related it being responsible in each horizontal band in the second case. If this were correct, the interference figures would likely be different, as demonstrated with figures 18(a) and (b), but would have to be problematic, which obviously is not the case in the two cited examples. Nevertheless, the fact remains that this unequivocalness occurs only in the horizontal sections with parallel side walls (compare fig. 12) and even then only for the pure wedge field, not generally. Furthermore, unequivocalness occurs only in the zones in which the two systems intersect. In all other cases, the possibility of double or ambiguity can be counted on. The latter may happen when several such fields lie close to one another so that the light from the slit can cover them.

However, this phenomenon need not entail difficulties in practice, since in general fields the contrast yield of one system so predominates that the other scarcely appears; if it does, it is almost always possible to identify the two systems as such and to distinguish them. The quantitative interpretation of the field can then be made by proceeding with one of the systems and disregarding the other completely. If desirable, a change-over from one to the other can be effected in the intersection points, while still preserving the connection. It follows that the quantitative interpretation can be made without it being absolutely necessary to have both systems available. For this reason, a further investigation into the final cause of the minor discrepancy between theory and experiment, as indicated in figures 18(d) and (e), was omitted for the time being.

The general conclusion is that when the interference slit is used the interference figures do not indicate lines of equal density but lines of equal density increase or decrease referred to the particular border of the examined zone, measured normal to the interference slit. However, these lines are likely to vary angularly and abruptly within a width of 0.5λ, even with continuous object field and density variation, owing to the zonal separistic behavior in conjunction with the fluctuation width of 0.5λ illustrated on the "Swiss Cross" for the appearance of the first band at the zone boundary. (Compare section 4.)

This result was confirmed on various random fields. (Compare figs. 8 and 9.) It was also found that, in the sense considered here, not only opaque object field boundaries are feasible, but also discontinuities of the density within the object field, such as compression shocks in supersonic flows, and areas of maximum and minimum density or reversal points, for example. One such phenomenon at extreme densities from the appearance of different band systems is particularly perceptible in figure 21(d).

4. INTERPRETATION OF INTERFERENCE FIGURES

(a) Preliminary Remarks

There is no intention of going into details about the general theory of interpretation of interference figures, since ample literature on the subject is already available. The same applies to the special interpretation of rotationally symmetrical systems which also have been treated extensively elsewhere, nor is it intended to submit rational interpretation schemes. The purpose is rather to devote particular attention to the characteristic peculiarities for the present method and hence to guarantee the junction with the conventional methods. The problem is therefore simply an attempt to ascertain how figure of lines

of equal density can be constructed from interference records obtained by interference slit with or without artificial superposition of a wedge field. Everything else comes within the scope of ordinary interferometry and can therefore be discounted.

At the end, several patterns of various interference records are added, some without detailed discussion, simply with the intention of giving an idea what this method is already able to do at the present state of development.

Unfortunately, the writer had no Mach-Zehnder interferometer at his disposal, hence was unable to compare the records made by both methods under otherwise identical test conditions. It would be gratifying if such opportunity presented itself some way or another in the near future.

(b) General Density Fields

As a rule, the interpretation of a completely unknown field requires four photographs, two interference photographs, I and II with mutually rotated slit and two schlieren photographs, I(a) and II(a) with schlieren edges whose direction is equal to that of the employed slits. In the majority of cases, it will be advisable to let the slits form a 90° angle with one another. The necessity for two interference photographs results from the fact that each zone normal to the slit leads, so to say, its own independent lift, and is no way dependent on the adjoining zones. One of the photographs serves to connect all zones of the other photograph in one arbitrary cross section. But, since the band systems give no indications of whether the transition to the next band was accompanied by a density increase or decrease, the schlieren photographs responsive to density gradients must make the decision regarding this possible.

Fundamentally, however, it likewise is possible to take interference photographs I(b) and II(b) with slit displaced relative to setting I and II instead of schlieren photographs. The local gradient is then deduced from the fact whether the band spacings are greater or lesser.

If the qualitative gradient field in the interference images I and II is known, it is advisable to fix one arbitrary line each as zero line and proceeding from it provide the whole network of bands with successively increasing or decreasing numbers $\overline{n}$ depending on the gradient.[1]

Next follows the measurement in image I of the abscissas x of the different bands normal to the interference slit for as many ordinate

---

[1]Hereafter n denotes the number of bands and numbering, not the index of refraction.

values y as parameter, as seems necessary within the ambit of desired accuracy. It is advisable to let the zero point of the abscissa coincide with the ordinate so that the latter covers the entire field height as much as possible and runs perpendicular to the interference slit II.

Then the obtained values $\bar{n}_I$, reduced by the eventual, artifically superposed wedge field from gradient $\Delta\bar{n}_I/\Delta x = n'_I$, are plotted in the form

$$n_I = f_I(x,y) = \bar{n}_I(x,y) - n'_I \tag{11}$$

and $n_{0I} = f(0,y)$ determined from the interpolation for $x = 0$.

Then the image II is evaluated on the basis of the same system of coordinates; the task can be limited to measuring the ordinates y of the identically numbered bands for $x = 0$, that is, $\bar{n}_{0II}(0,y)$ and, after subtraction of the eventual artificially superposed wedge field from the gradient n'_{II} in the form

$$n_{0II} = f_2(0,y) = \bar{n}_{0II} - n'_{II}y \tag{12}$$

represented graphically or in tabular form.

This then corresponds to the existing conditions; n_{0I} is then corrected so that $n_{0I} + \Delta n_0 = n_{0II}$.

So the final result is the desired variation of the lines of constant density according to the relation

$$n(x,y) = n_I(x,y) + \Delta n_0(0,y) \tag{13}$$

The density field itself can then be determined by plotting the field or by further treatment from the tabulated designs in the customary form of normal interference photograph.

If the object field presents discontinuous pressure jumps, as frequently occurs in supersonic flows with the appearance of compression shocks, each one of the areas separated by an unsteady density variation must be treated separately. In many cases, the mutual connection can be found by the use of white light with the aid of the so-called 0-line.

In each case, for determination of the absolute density level, as for ordinary interference photographs, knowledge of the absolute density in all separated fields not coordinate with known fields, at least in one point, is required. What fundamental possibilities the use of white light in this particular method affords, perhaps by fitting small auxiliary cameras next to or in the object field, has not been investigated so far.

(c) Fields of Disturbance and Normal Flow Fields

Fields of disturbance are defined as such objects in which in all zones perpendicular to the interference slit a great percentage is covered by a constant density field, and a comparatively small portion is taken up by a variable density field on which in no way the condition of small variation needs to be imposed. In such a situation, the center of gravity of the vector diagram of all zones exhibits almost the same direction, with the result that a normal picture of lines of equal density appears, whose interpretation in this respect requires no special comment. Hence, it is not necessary to take two photographs with mutually rotated interference slits.

An identical or similar situation is frequently encountered with flow photographs, especially on models and where often comparatively great areas of exact or sufficiently approximate undisturbed and known flow occurs. But, even if the areas of equal density are not large enough to produce lines of constant density, it may prove superfluous to make two photographs with rotated interference slit if a cross section can be found that reveals constant density or a known variation and overlaps the various zones. The interpretation is then made again the same way as described above. At times, one of the cited situations can be produced by appropriate overlap of a wedge field.

5. EXAMPLES OF INTERFERENCE PATTERNS WITH SOME EVALUATION RESULTS

The subsequently described examples are intended to give an idea regarding the quantitative feasibility of the method and the quality of the records obtained so far in comparison with phase-contrast and field-absorption records under all kinds of conditions as well as to demonstrate the method used by the writer in manipulating the photographs for obtaining quantitiative data.

Moreover, it should be noted that the experimental equipment available was rather limited, that is, actually comprising only a normal

schlieren optics with a spherical mirror subjected to errors of as much as three wave lengths toward the rims. The wind-tunnel disks likewise were subject to irregularities of up to several wave lengths and, on top of that, were mounted in such a way that they were exposed to high mechanical and thermal stresses which could be distinguished in each test. Consequently, in principle, comparable results still showed certain discrepancies which, in the writer's opinion, are solely due to the secondary circumstances, not to the method. This also applies not in the least to the first two subsequent examples on object glass for the comparison of which Michelson interferometer photographs were employed and which had been obtained under primitive conditions as already stated elsewhere.

In order to eliminate every conceivable source of error or uncertainty, the first phase of this method was carried out with two glass plates as object. The first, the so-called "small object glass," 2.6×3.4cm, is a sector of a normal microscope objective; the other, the "large object glass," is a 3×6cm sector from an ordinary, cleaned-off photographic plate. The comparative photographs were taken with a Michelson interferometer of 2.5×2.5cm field of vision, followed by synthesis of the partial figures to a unit.

Figures 21 and 22 represent the field absorption and schlieren photographs with vertical and horizontal slit for both object glasses. The appearance of interference lines in the bright areas of the small object glass on the schlieren photographs is of interest. It is a kind of one-sided dark-field effect which can be produced direct with every schlieren optics if a suitably narrow slit is used as light source. This is the same phenomenon described by Gayhart and Prescott (ref. 6). Figure 21(d) is a typical example of two intersecting systems of lines, which are easily separated in the lower half. The data used in the evaluation were inked in and numbered, the second, by way of illustration, was added as dashed lines in the lower half. Another system, inked in and numbered is shown in figure 22(c). Both photographs, figures 21(d) and 22(c), were measured during the evaluation over the entire field and, according to the rule for evaluation in section 4, the interpolation values for defining Δn along the three plotted lines were read from the graphical representation. In principle, the reading along one line is sufficient; the purpose of reading along three, in this instance, was to demonstrate the degree of accuracy of the Δn determination reproduced in figure 23. In figures 21(c) and 22(d), the blackenings are numbered only along the three intersection lines. Plotting whole line systems would have been impossible anyhow, in this instance, because the abrupt transitions of adjacent zones are already so pronounced that it is no longer a question of uniform system. However, no difficulties are entailed, as seen from the good agreement of the Δn values in figure 23, for the three sections obtained by combining the related n-values at the particular sections of figures 21(c), 21(d) and 22(c) and 22(d), in exact accord with the evaluation rule of

section 4. A constant was added to the difference formation at the individual sections in such a way that all three results have, in principle, an arbitrary point in common; it is the same as fixing the absolute level which, as stated elsewhere, is, in principle, indeterminate.

Again it is pointed out that the numbering of the lines and blackenings must be effected in closest cooperation with the respective schlieren photographs in order to recognize if and where it must be increasing or decreasing. Incidental to the Δn values of figure 23, it should be noted that the fact that they carry the fluid character of a curve is merely to be taken as exception. In principle, the Δn variation can, of course, be abrupt, hence it is not justified to strike an average by plotting a compensating curve. But it is well permissible and even advisable to average the Δn values obtained for identical abscissas along different sections.

The final result of the two evaluations on lines of equal density is represented in figure 24 together with the corresponding photographs obtained by Michelson interferometer in the Zeemann laboratory at Amsterdam. The agreement may be regarded as very satisfactory, considering the aforementioned inadequacies of the Michelson interferometer photographs.

A comparison of several photograhs on a Laval nozzle for $Ma = 3$ and their evaluation is represented in figure 25. In view of the large areas of practically constant density at the nozzle inlet and outlet, this object is very appropriate for field absorption as well as for phase-contrast photographs with vertical slit (figs. 25(a) and (b)), but of course only on the assumption that these two areas differ in the optical path length approximately by a whole multiple of a wave length. If this is not the case, there is a twofold possibility of inferior or totally useless figures. In the first place, if the interference slit is narrow enough so that the entire field of vision is practically evenly covered, the center-of-gravity vector can become very small, so that field absorption alone produces good figures, or in the second place, if the interference slit is too wide, each one of the two areas produces an independent interference field with the result that the lines in the central portion become vague or completely undefinable, even by the field absorption method.

For the photographs with horizontal slit (fig. 25(c)) and for overlapping of a wedge field (fig. 25(e)), the field-absorption method is definitely superior.

Schlieren photographs were not necessary in this evaluation, since the gradient variation was sufficiently known from pressure-distribution measurements.

The numbering in figure 25(a) is monotonic. But in the interest of image quality it is written out only there where the line density permits this easily.

As regards figure 25(e), it is readily apparent that the density variation plotted against nozzle length manifests an S-shaped character; so the superposition of an oppositely directed wedge field produces two areas in which the mutual gradients are inversely equal. The comparatively wide, fringeless areas appear. Since, after the overlapping, the newly created apparent density field changes the sign of the density with respect to the ends in the midportion between these areas, the numbering of the fringes must count backwards.

As a consequence of a contour error of the nozzle, the supersonic part of the flow, the compression shock, indicated by dashes in figures 25(a), (c), and (e), occurs, which in association with the nozzle contour divides the supersonic parts in four zones: I, II, III, IV. The Δn-relation for zone I follows from the fact that equal density (almost that of the atmosphere) prevails in section A. The same holds true for zone II, the measuring rhombus, if the density is everywhere constant and the level can be regarded as known, which is imputed here, by reason of the absence of lines (at zero slit setting). The Δn-relation in section B for zones III and IV is obtained from a combination of figures 25(c) with (a) and (e). The asymmetry is due to the superposition of a weak density field in figure 25(c). The level for these zones is, by way of illustration, so determined that the levels of zones III and IV are mutually equal in the objective point O of the four zones and equal to the mean value of zones I and II in this point. Such averaging was omitted in the present example because the small pressure increases accompanying the compression shock fell within the degree of accuracy desired in this experimental evaluation.

The result of the evaluations on lines of equal density is represented in figures 25(d) and (f). An originally intended direct comparison with the theory was omitted for two reasons. In the first place, it was found that the nozzle contour differed from the chosen form as a result of a systematic measuring error in manufacturing and so produced the compression shock. In the second place, the employed channel windows show stated but qualitatively not yet accurately determined irregularities, which in conjunction with the likewise unsatisfactory mirror produce errors of several wave lengths. As a result, the number of bands is not exactly (5 to 10 percent discrepancy) agreeable with that expected by theory; but the general variation of the lines is entirely satisfactory with theory.

Also of interest are the differences of the two evaluations. According to the writer's conception that obtained with superposed wedge field is more accurate, although its departure from theory is greater as regards number and position of bands, for it even shows slight flaws in the glass structure in the basically gradient-poor zones, to which the

zero setting already ceases to respond. From this, it can be concluded that it is necessary to investigate eventually defective glass with which one is forced to work with superposed wedge fields rather than zero slit setting, to define the variation exactly and take it into consideration in the evaluation. Furthermore, it is necessary to determine if and what temperature stresses occur during measuring, since it was found that they could be considerable and a function of the measuring time.

Figure 26 represents several variations of the method applied to a supersonic airfoil at Ma = 2.1, along with the graphical presentation of the lines for the purpose of evaluation of three different cases. With slit turned through 90°, the evaluation in first approximation required no corresponding photographs, since the center-of-gravity vector in the entire figure is likely to be controlled by the comparatively wide field of constant density before the airfoil and, even if this should not hold true for the entire field, it would still be applicable to the very small half profile height, to which the evaluation can be limited. For the aim of the evaluation is not, as in the previous example, to find the system of lines of equal density, but to define the pressure distribution on the airfoil for the purpose of comparing it with the theoretical variation. The results of figure 27 was discussed without going into further details. The theoretical curve is shown as solid line. The test points indicate a very gratifying agreement with theory up to the separation point on the airfoil. The greatest number of points and the relatively little scattering indicate, as was to be expected, the overlapping of the negative wedge field (in flow direction), whose gradient is in the same direction as the field in question. The superposition of a positive wedge field is entirely unsuitable in the present case, since only two or three test points are obtained then. The number of test points at zero slit setting is less and scattering greater than with negative wedge field. Whether the variation after separation of flow (chain-dotted line) was correctly reproduced, seems problematic, since the extent to which the outer field may be continued through the dead water between sound flow and profile contour is not guaranteed. But this is an aerodynamic rather than an optical problem and therefore not explored further.

The airfoil test data are comparatively very favorable as regards accuracy and mutual comparability and theory. This is undoubtedly due to the smallness of the object field, especially in contrast to the previously described nozzle measurement, with the result that the errors of the mirror and the channel plates can be disregarded.

Lastly, figure 28 represents three complete sets of photographs of airfoil flow measurements as illustrative examples. They require no special comments, except one concluding remark. For economical reasons, it proved expedient to combine the photographs in groups and to make

collective productions from great enlargements, which, however, did not benefit the visible contrasts any. The reader is therefore requested to bear in mind that the originals show better contrasts than the copies shown here.

6. EXPERIMENTAL SETUP

A brief summary of the experimental setup (figs. 29 and 30) follows.

Obviously the coincidence method is involved here. The light source is a water-cooled Philips-maximum pressure-mercury lamp from which light of a certain wave length ($\lambda = 0.54\mu$) was screened out for use with the aid of a double monochromator; however, it was found that a Kodak-filter No. 77 itself produced acceptable fringes.

After passing the monochromator, a picture of the monochromator entrance slit is formed in the plane L with the aid of a condenser. This is then the slit that serves as active light source of the actual optical setup. Directly behind, a miniature mirror, 4 mm in diameter, deflects the light 90° in direction of the object field or spherical mirror. The latter is mounted in such a way that the light source is slightly excentrical to its axis of symmetry at the distance of the radius of curvature of this mirror. By this method, the diffraction pattern B is formed at the same distance reflective to the axis of symmetry, and where the schlieren edge is placed for the schlieren method and the interference slit when the interference method is used. The optics mounted directly behind it forms then the desired schlieren or interference pattern of the object plane on the ground glass S.

It is true that the coincidence method has the drawback that a not completely identical course of the reciprocal light beams may at times result in double pictures or at least in reduced sharpness. Besides, the glass plates bordering the object field produce very disturbing reflexes occasionally. A parallel light in the object field and one passage of light would be preferable, in principle, in view of the greater possibilities for the proportions of the light source. In spite of that, it still seemed necessary to apply the coincidence method, since, owing to the smallness of the supersonic wind tunnel with its $3 \times 3 cm^2$ test section available for flow investigations, a second passage of light was necessary to assure a somewhat useful number of bands. With greater working sections or by working with higher static pressure, as intended in future tests, the conditions will be much better in this respect. The other setup can then be used immediately.

For flow studies, the small supersonic tunnel (fig. 31) placed directly in front of the spherical mirror, forms the object plane, while

for the other more basic tests, the plane 0 (fig. 29) is used as such. The image field varies in the various tests and may amount to 25cm diameter corresponding to the mirror radius, which matches the corresponding minimum dimensions of the light and interference slits, according to equation (3b). Concerning the latter, it is quite conceivable, especially with a single passage of light through the object field that eventually light and interference slits placed parallel at proper distance from one another will be used, because then there is no danger of doubling. Thus, the brightness of the picture could be increased and the exposure time kept short.

Translated by J. Vanier
National Advisory Committee
for Aeronautics

REFERENCES

1. Zernike, F.: Physica 9, nos. 7 and 10, 1942.

2. Zernike, F.: Roy. Astron. Soc., March 1934.

3. Burch, C. R.: Roy. Astron. Soc., March 1934.

4. Linfoot, E. H.: Proc. Phys. Soc. London 58, 1946 . . . .

5. Köhler, A., and Loos, W.: Naturwiss. 29, Heft 4, 1941.

6. Gayhart, E. L., and Prescott, R.: J. Opt. Soc. Amer. 39, July 1949.

7. International Critical Tables, vol. VII (National Research Council of the U.S.A.).

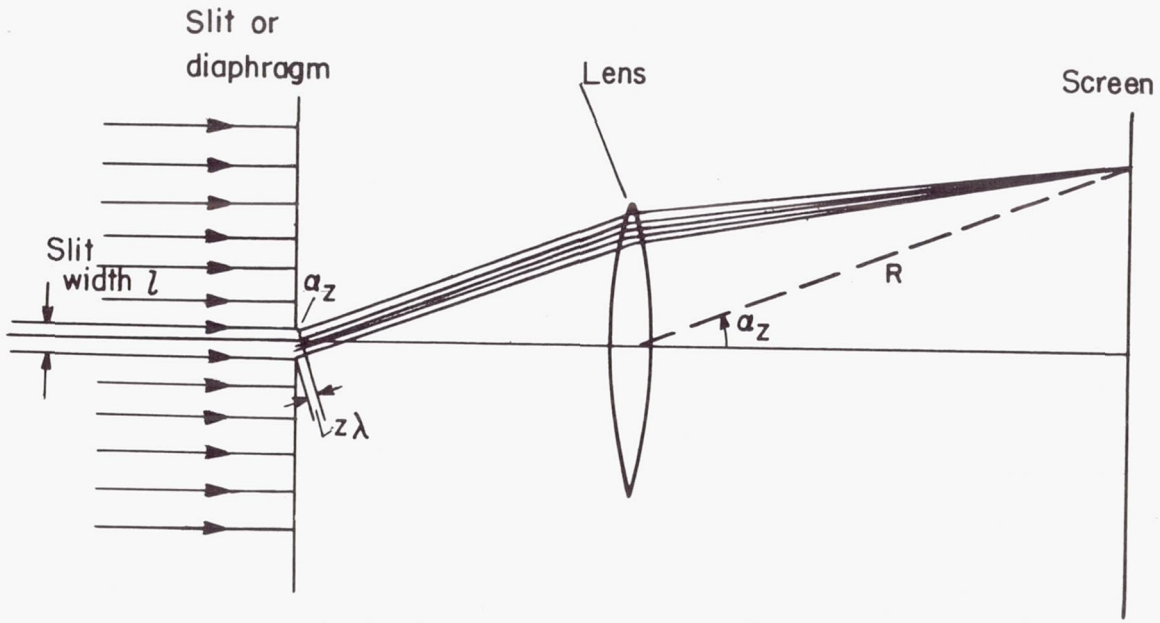

Figure 1.- Formation of diffraction pattern for a slit.

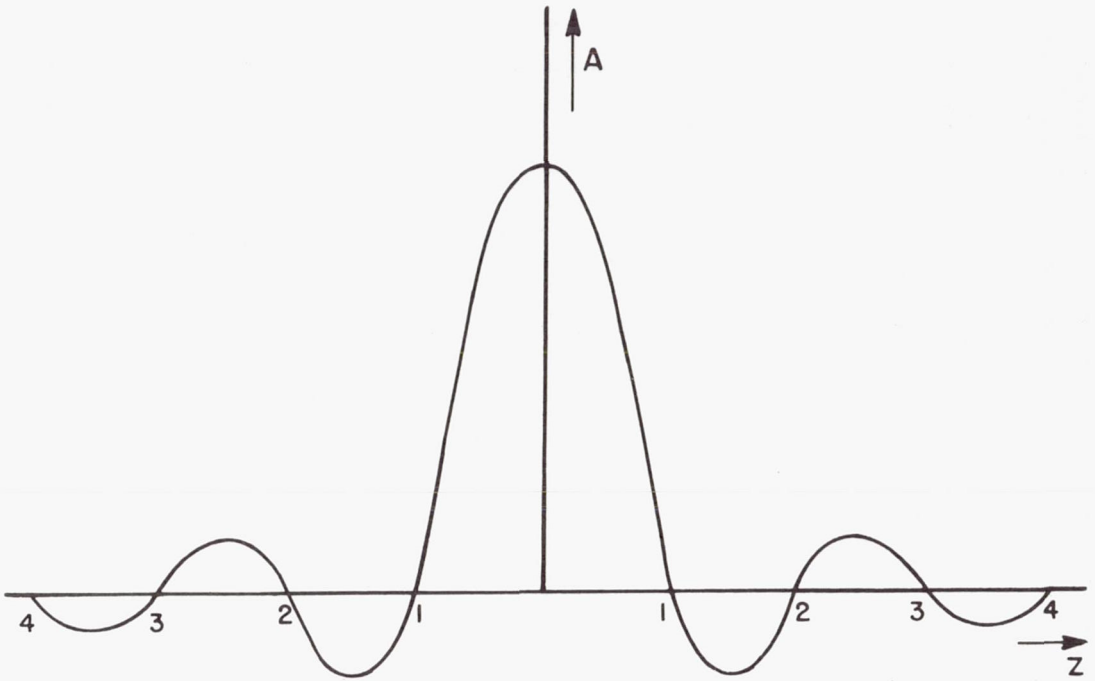

Figure 2(a).- Amplitude distribution of diffraction pattern at the slit.

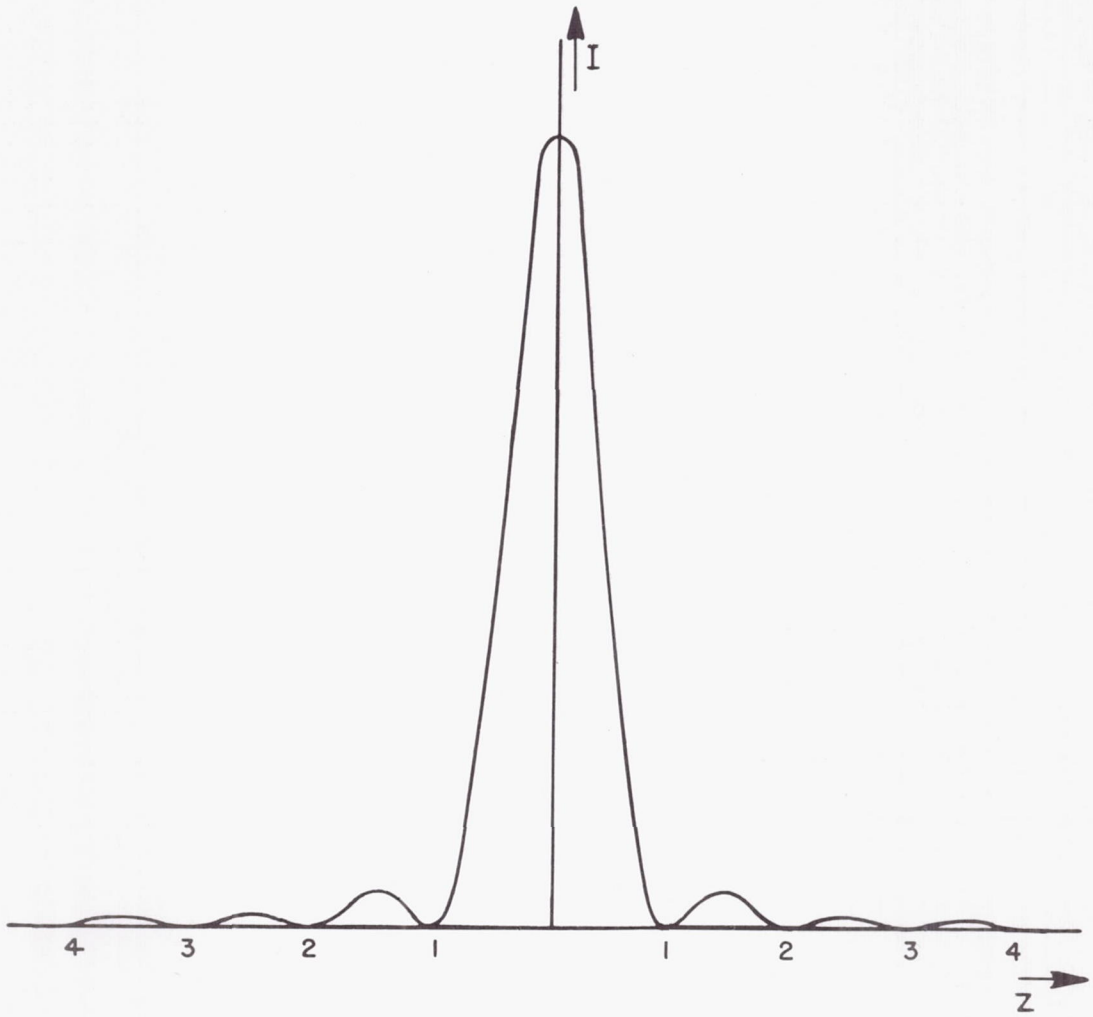

Figure 2(b).- Intensity distribution of diffraction pattern at the slit.

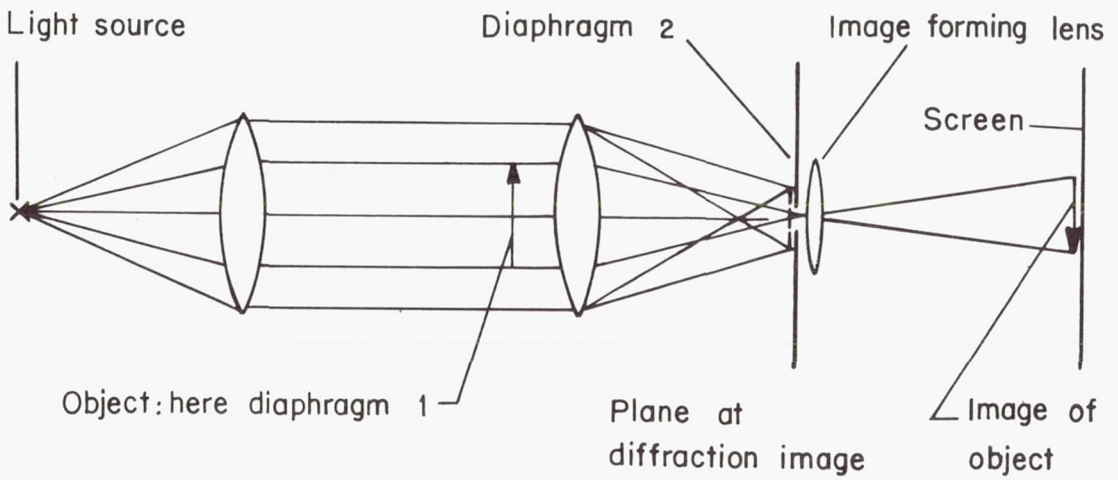

Figure 3.- Illustration of a diaphragm by means of a lens of variable aperture.

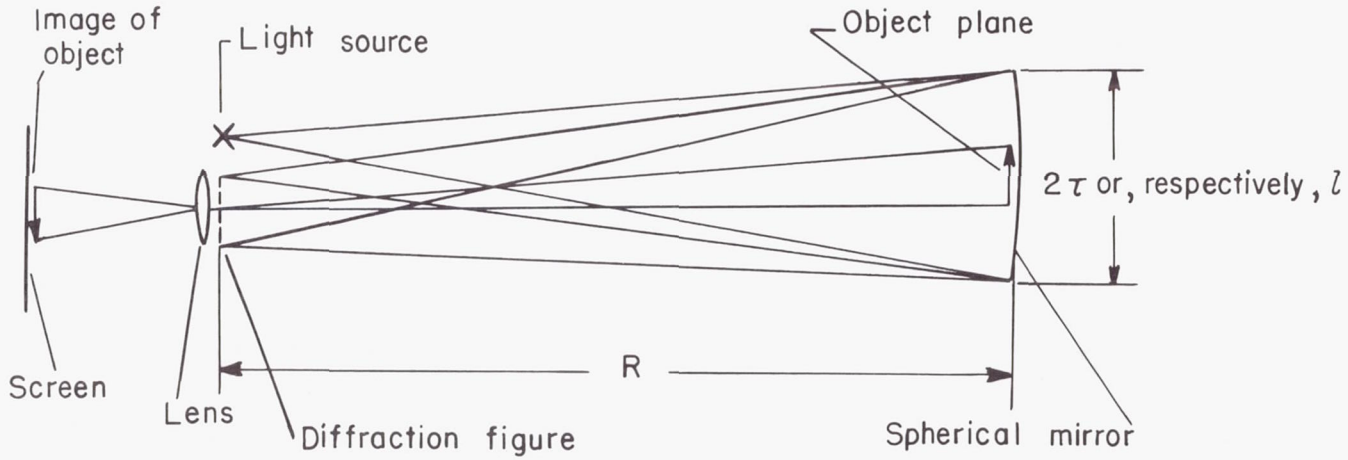

Figure 4.- The coincidence method.

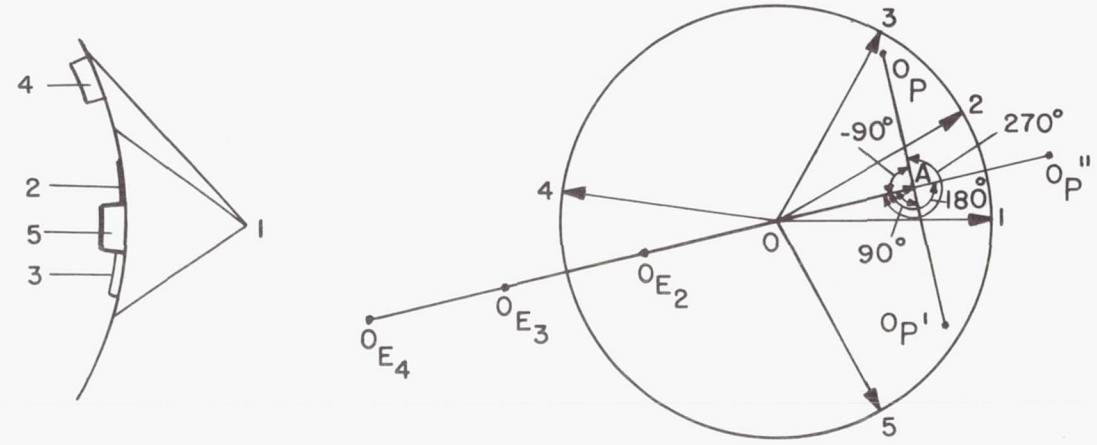

a : Plane of object

b: Vector diagram

Figure 5.- The vector diagram of the object plane.

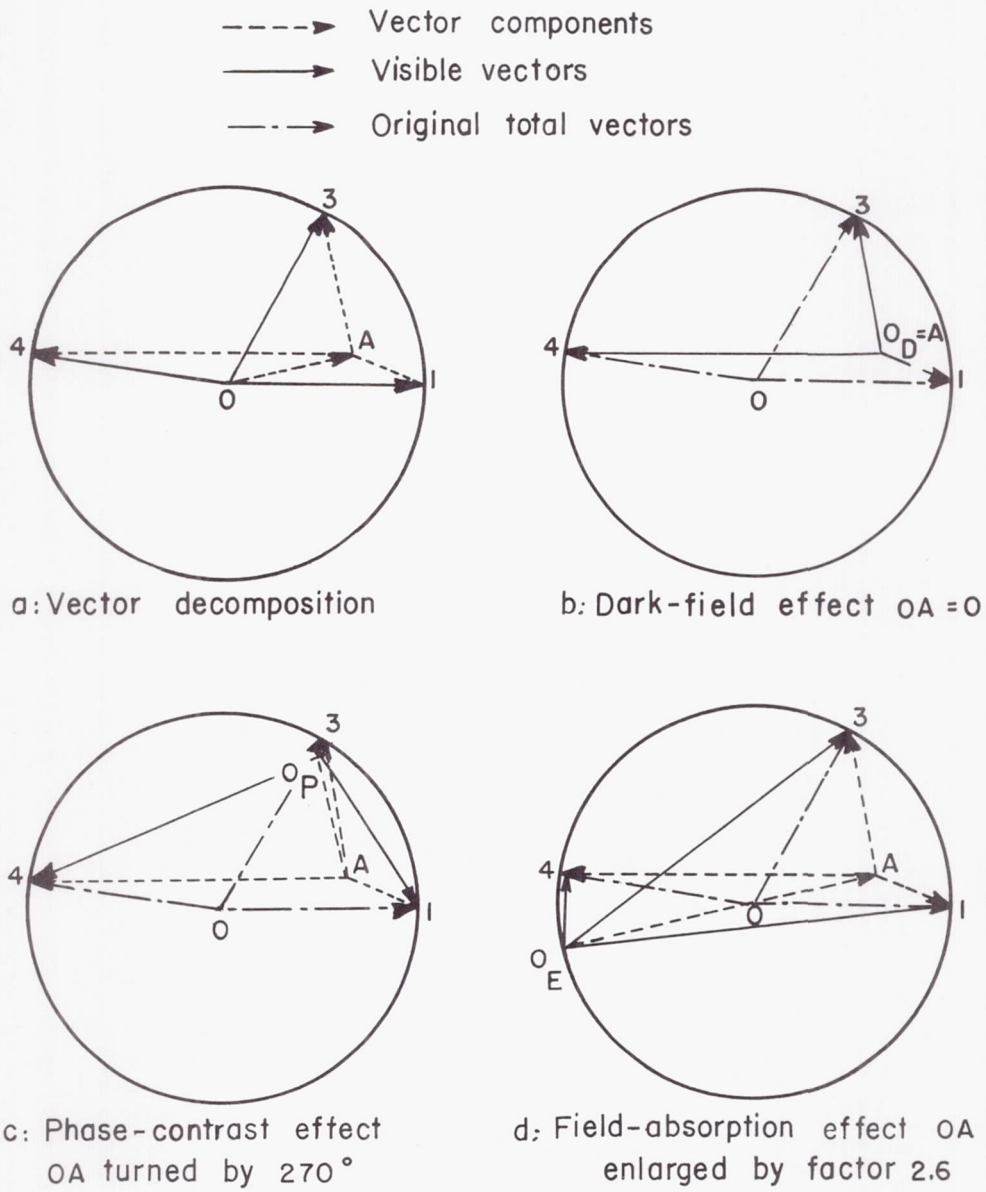

Figure 6.- Geometric representation of various interference effects.

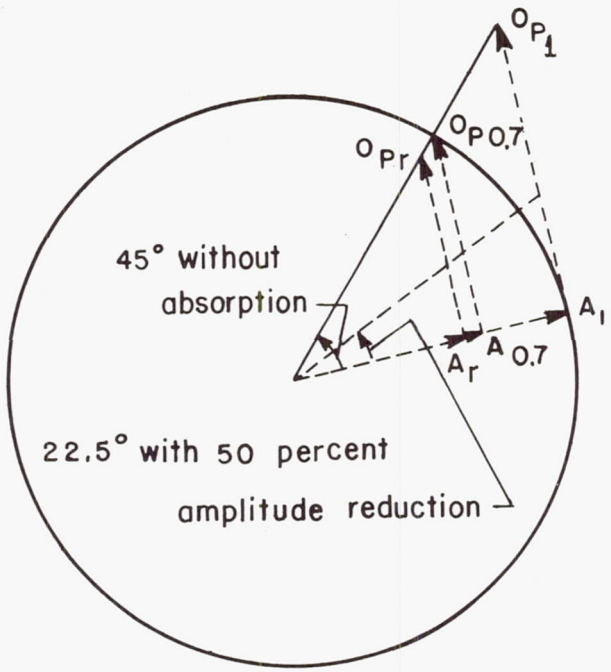

Figure 7.- Discussion of phase-contrast effect.

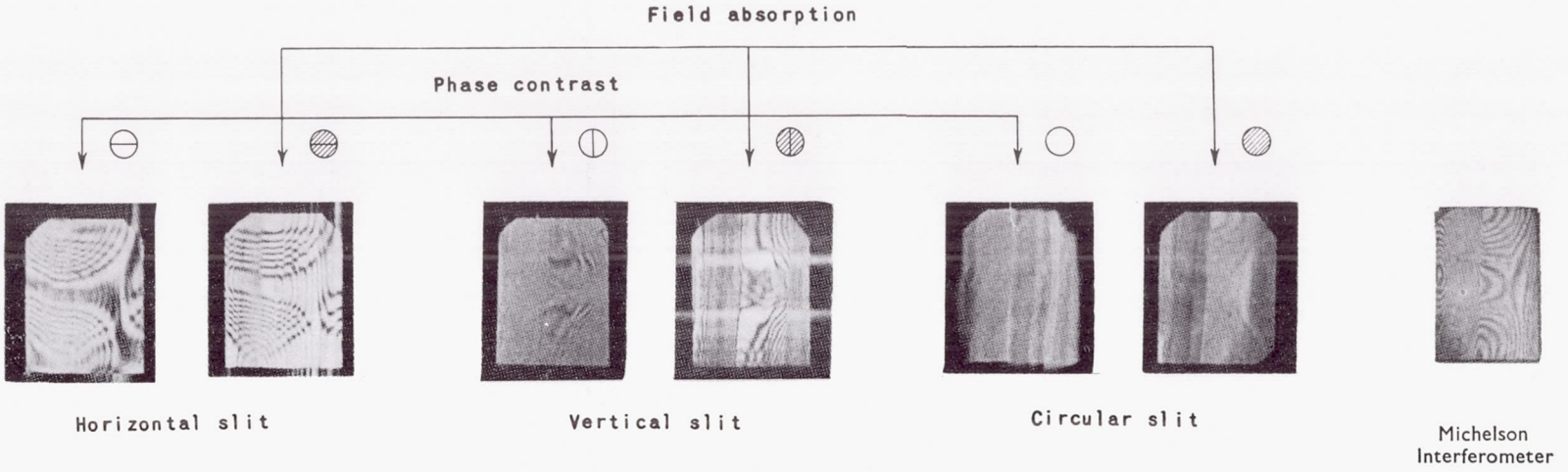

Figure 8.- Various interference phenomena at the small object glass.

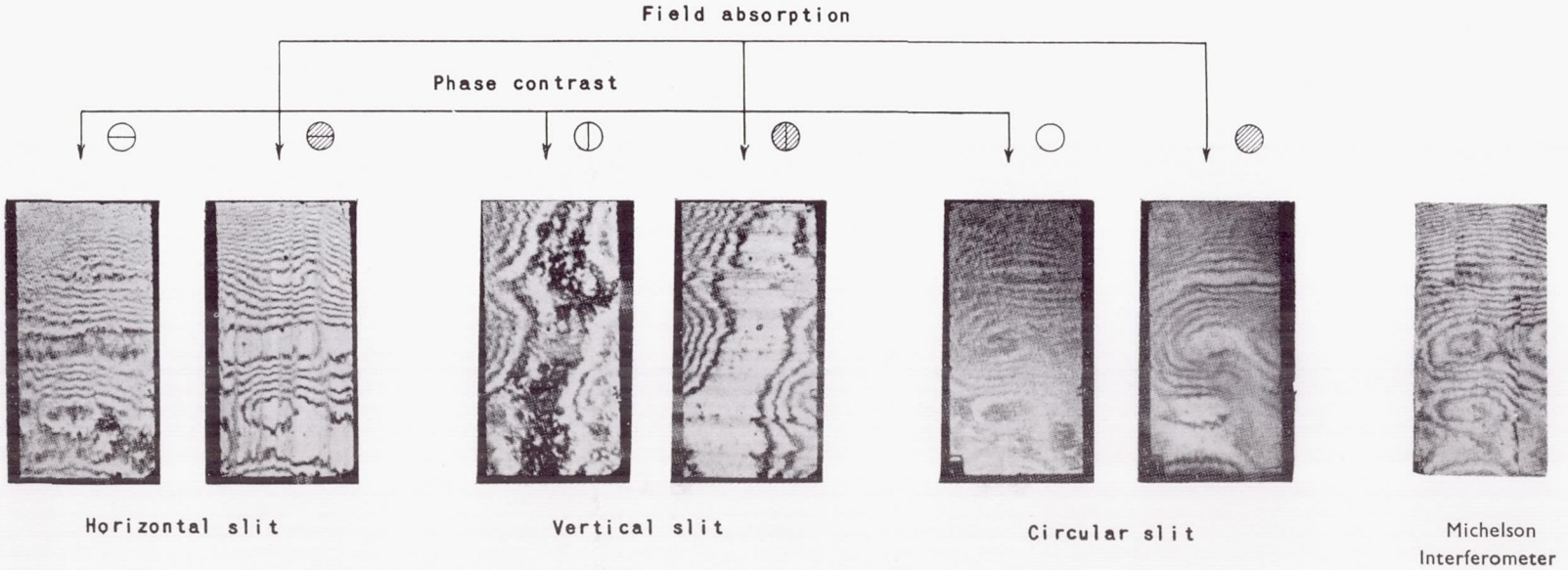

Figure 9.- Various interference phenomena at the large object glass.

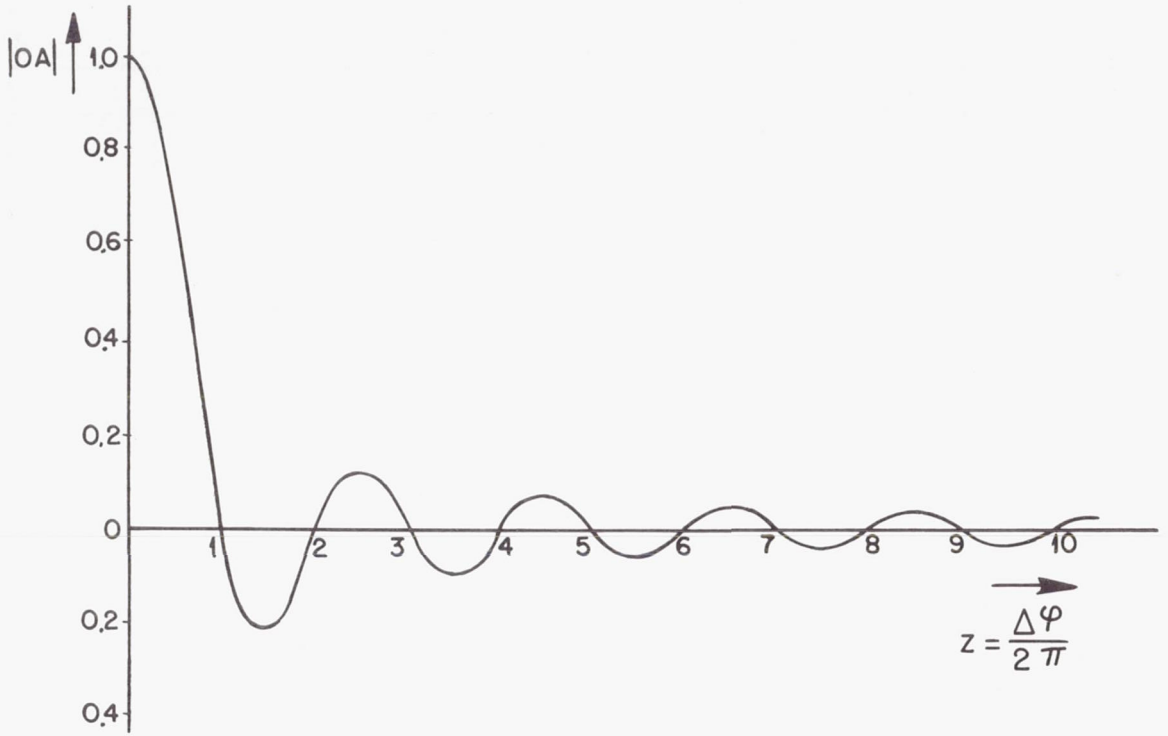

Figure 10(a).- Center-of-gravity vectors of several wedge fields plotted against total phase difference of both border zones.

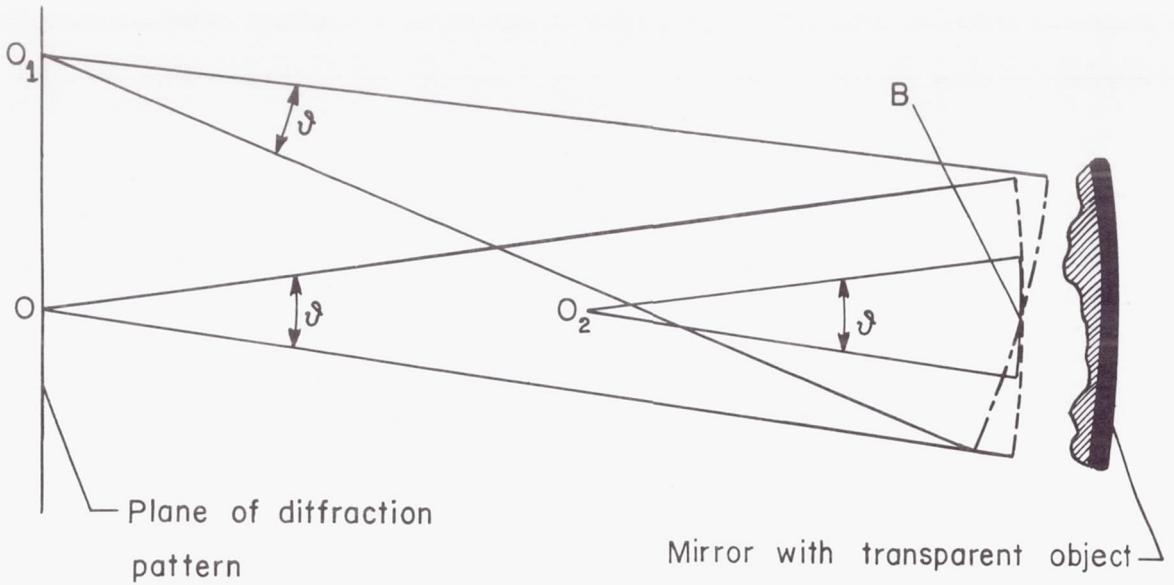

O = center of curvature of mirror (interference slit at zero setting)

O_1 = position of interference slit for wedge field superposition

O_2 = position of interference slit for superimposing a convex field

B = spherical shells or cylindrical surfaces near the mirror in which the effective vector diagrams can be constructed

Figure 10(b).- Possibilities of field superpositions.

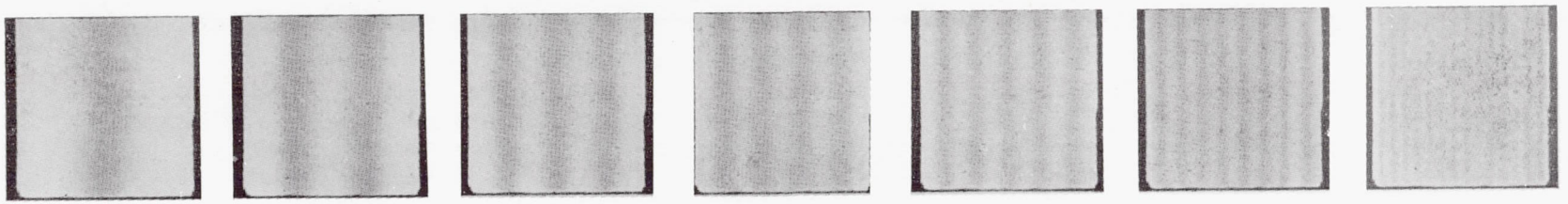

Figure 11.- Variable, apparent wedge field produced by field absorption in gradient less object field with edges parallel and vertical to interference slit.

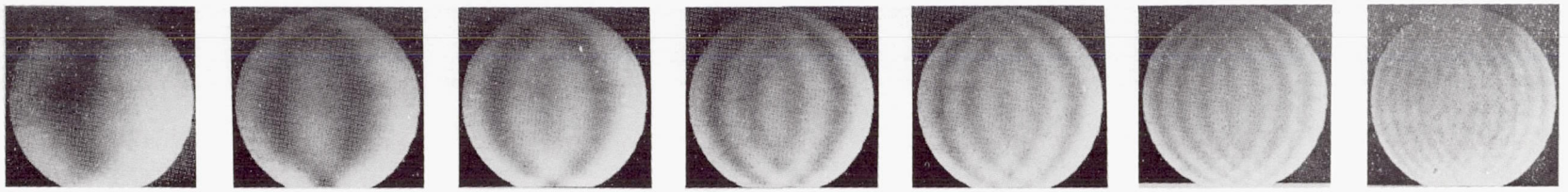

Figure 12.- Variable, apparent wedge field produced by field absorption and interference slit on circular object without gradient.

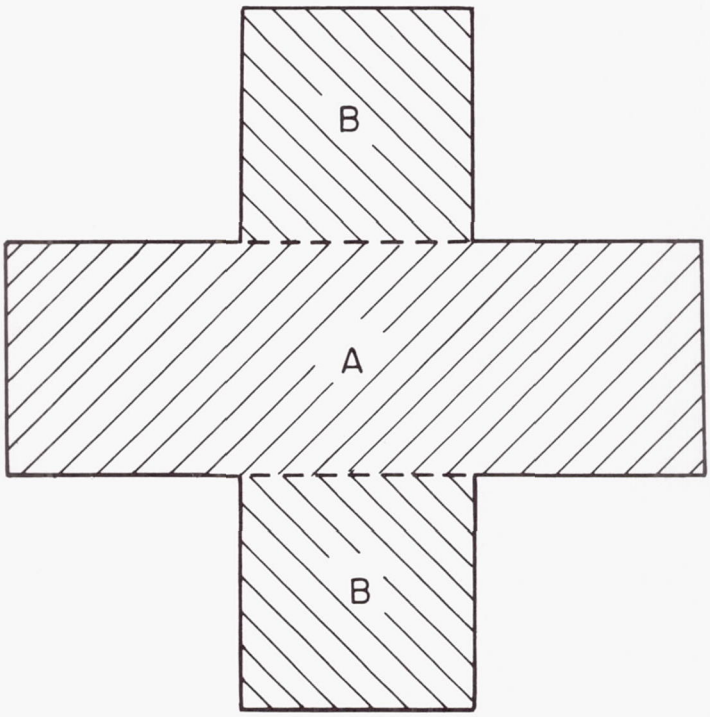

Figure 13.- "Swiss cross."

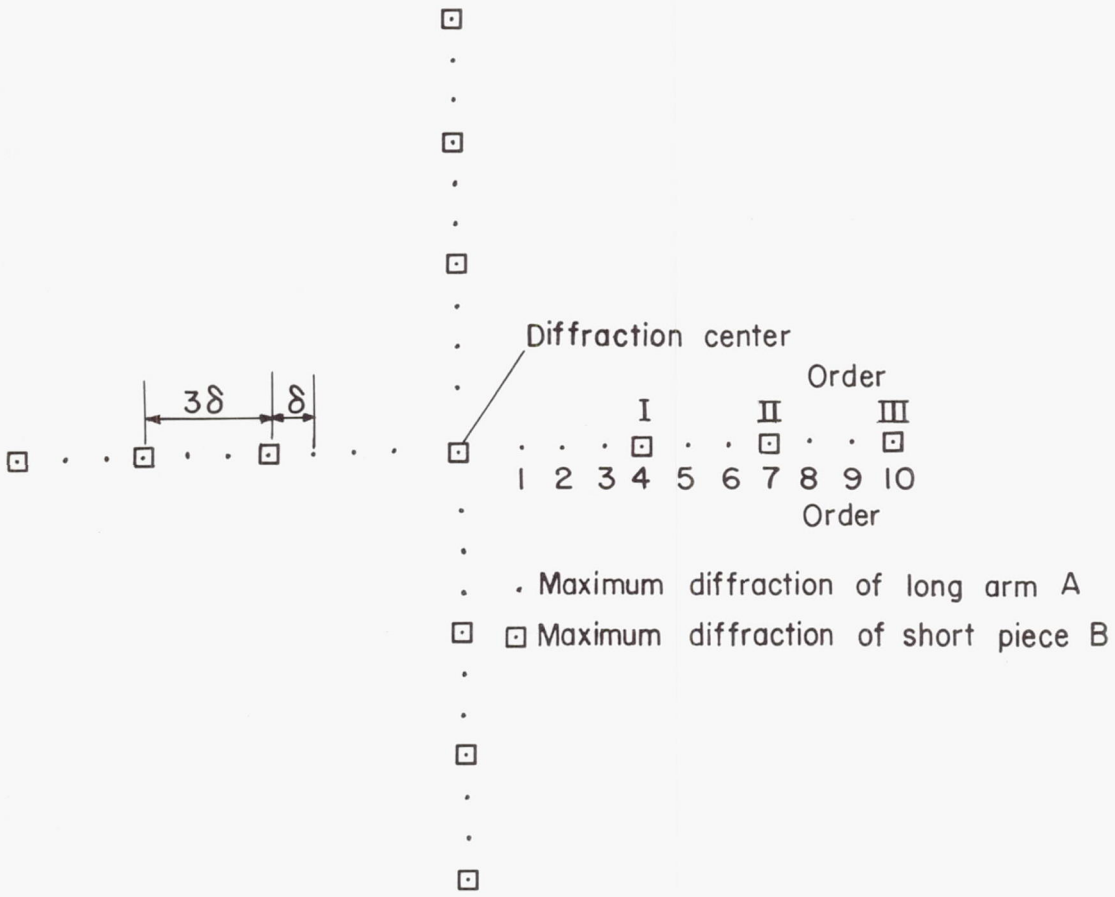

Figure 14.- Global diffraction figure at the "Swiss cross."

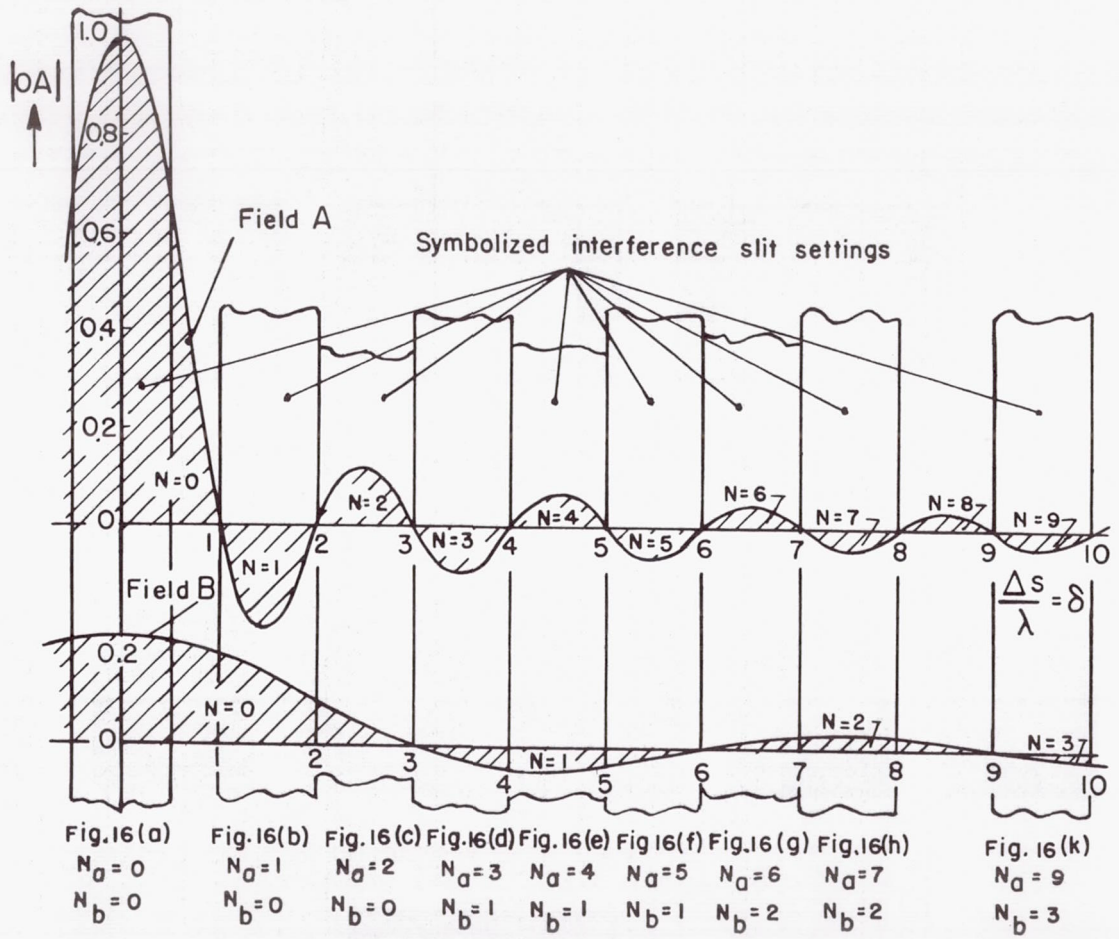

Figure 15.- Amplitude distribution of superimposed diffraction figures on the "Swiss cross" with various slit settings. n = number of apparent blackenings.

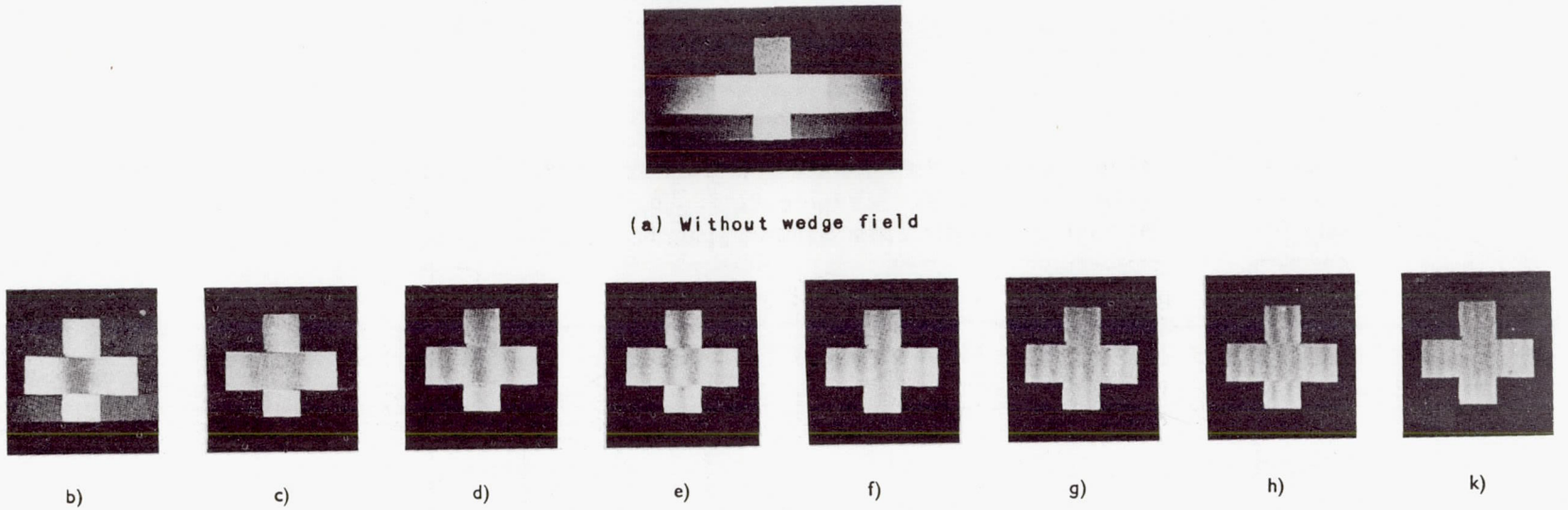

Figure 16.- "Swiss cross" illustrated via slit and field absorption with and without variable wedge field.

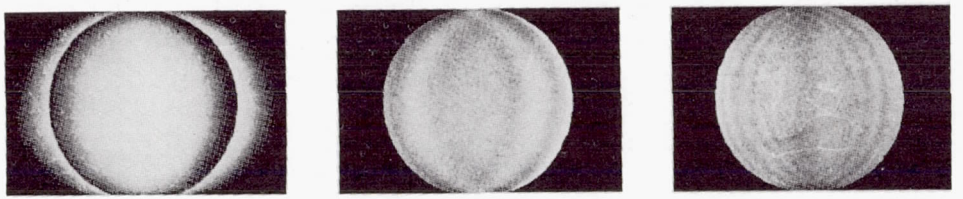

Figure 17.- Phase-contrast image of the circular figure with variable wedge field.

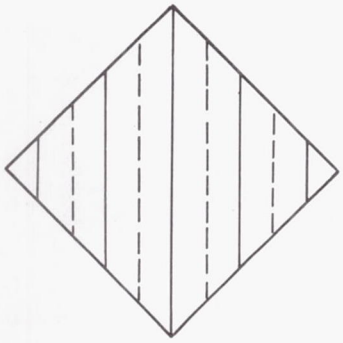

(a) Lines of equal density in the rhombus

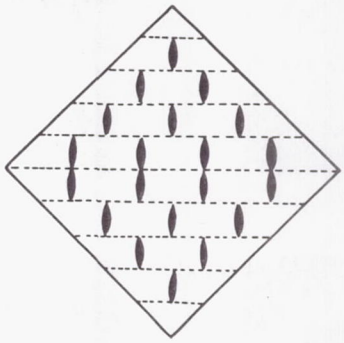

(b) Interference figure in the rhombus according to center-of-gravity vector concept for the interference slit (field absorption)

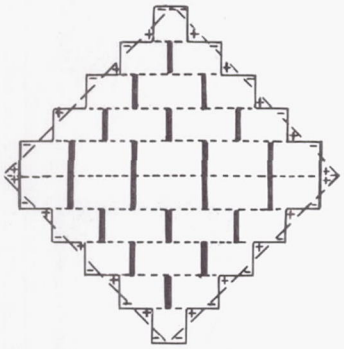

(c) Interference figure in the step contour according to center-of-gravity vector concept for the interference slit (field absorption)

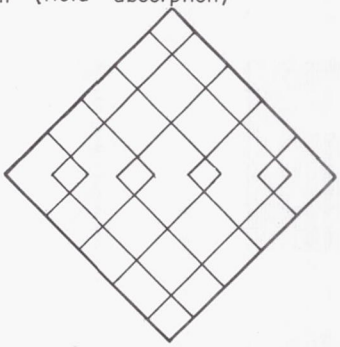

(d) Theoretical interference figure in rhombus for interference slit (field absorption)

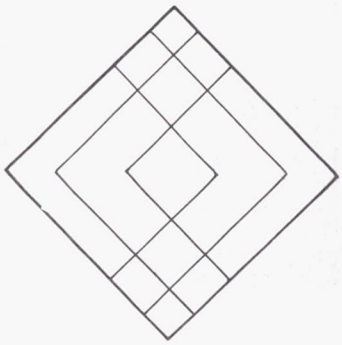

(e) Experimental interference figure in the rhombus for interference slit corresponding to figure 19 (field absorption)

Figure 18.- Discussion of interference figures in the rhombus with wedge field.

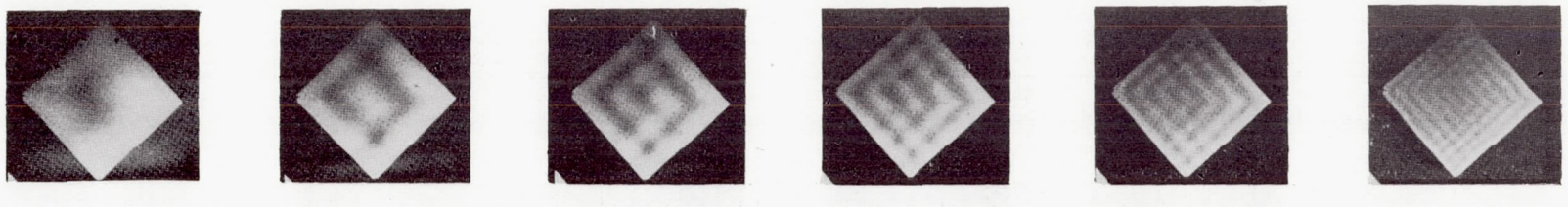

(a) Large rhombus

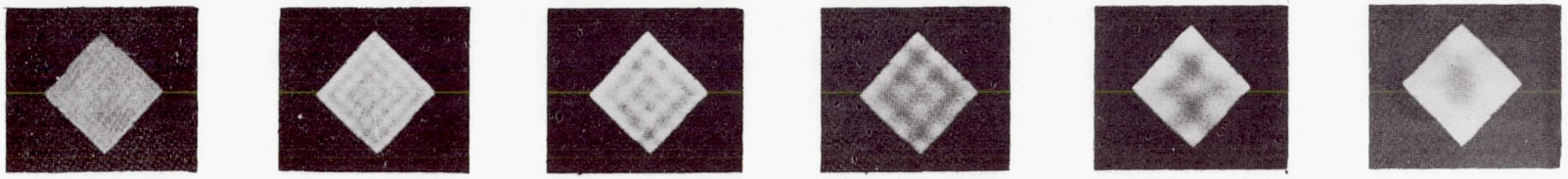

(b) Small rhombus

Figure 19.- Rhombus with wedge field figured via slit and field absorption.

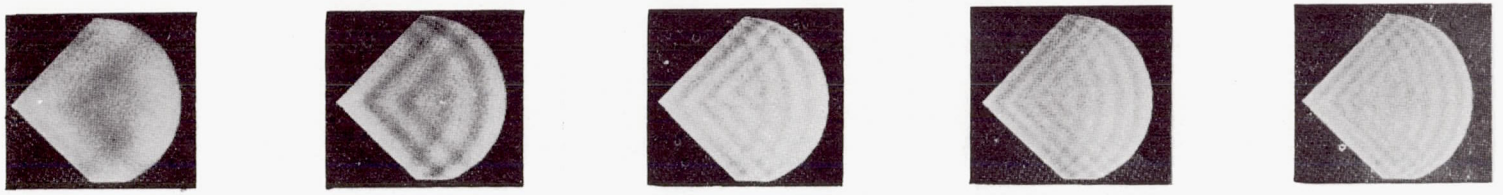

Figure 20.- Semicircular rhombus with wedge field via slit and field absorption.

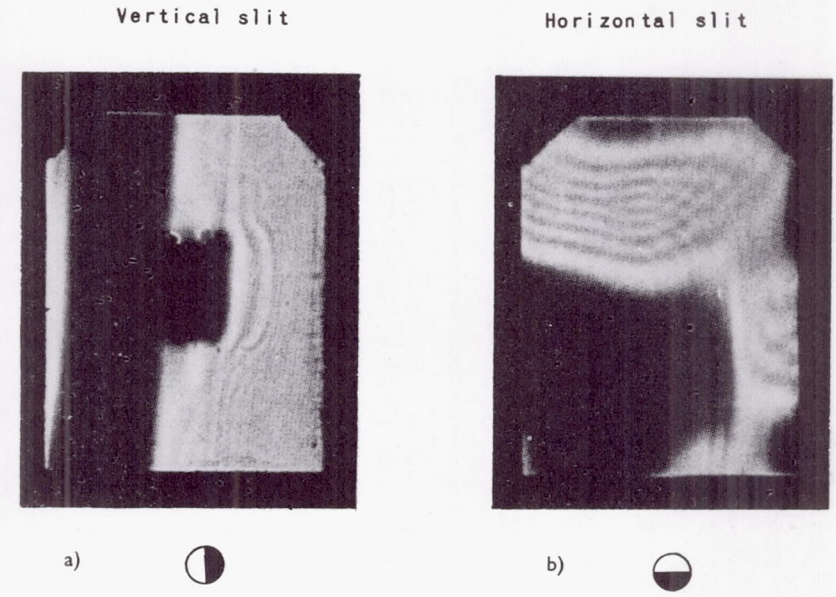

Figure 21.- Interference photographs by field absorption, small object glass.

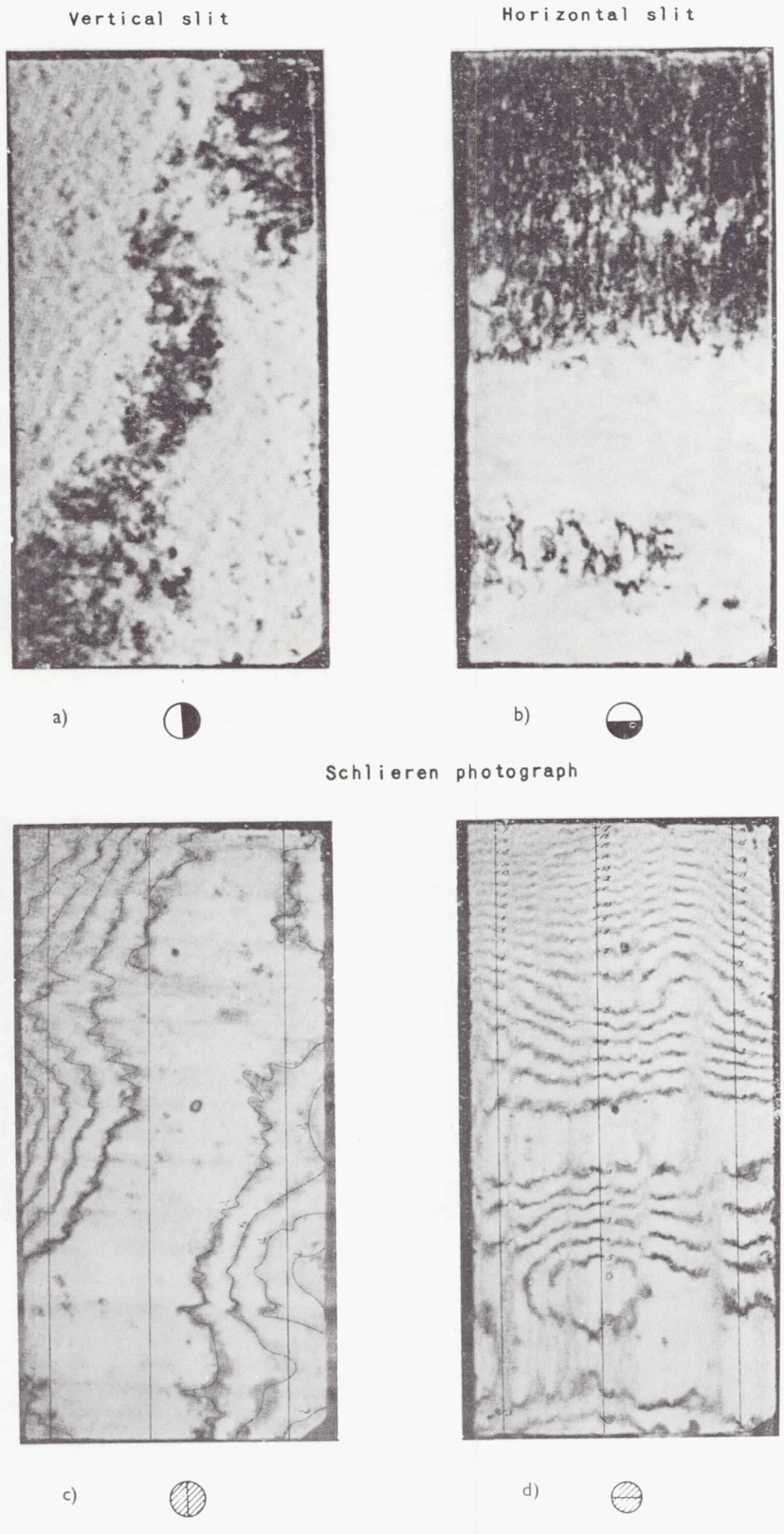

Figure 22.- Interference photographs by field absorption, large object glass.

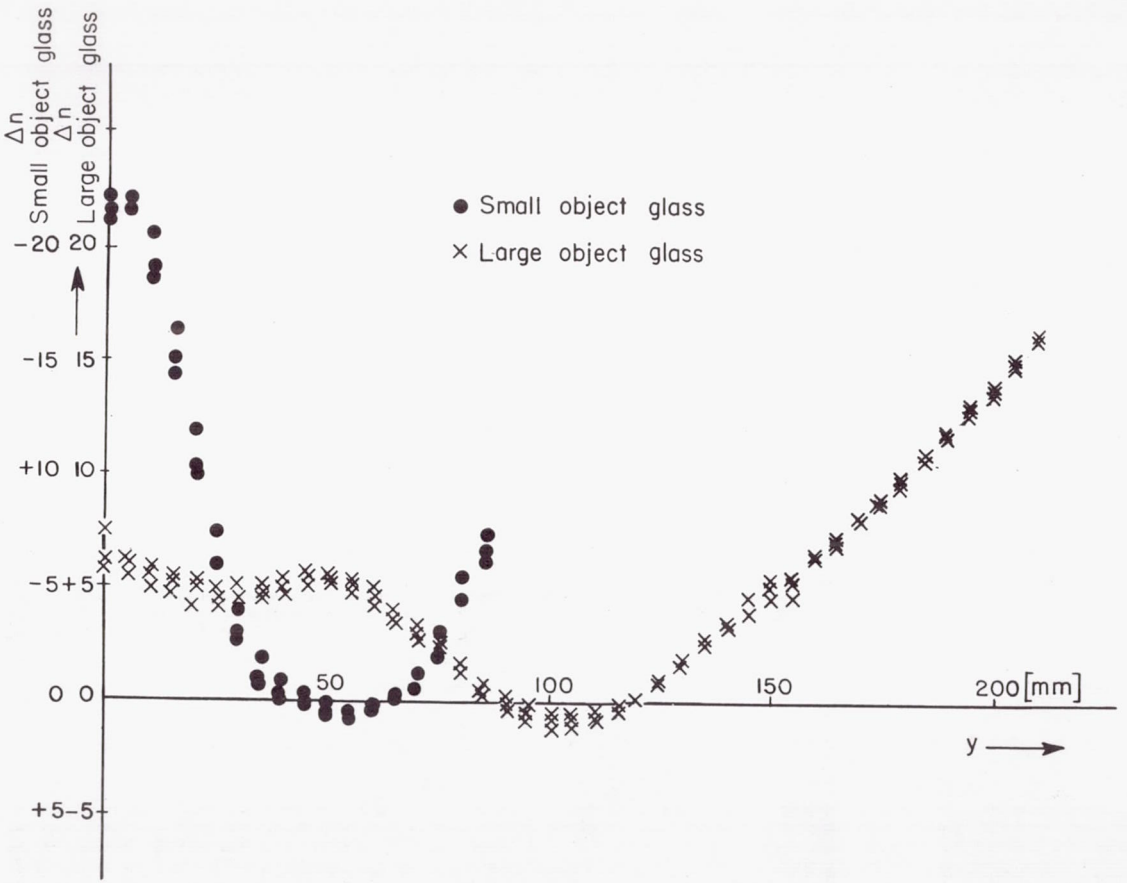

Figure 23.- Δn-variation of object glasses.

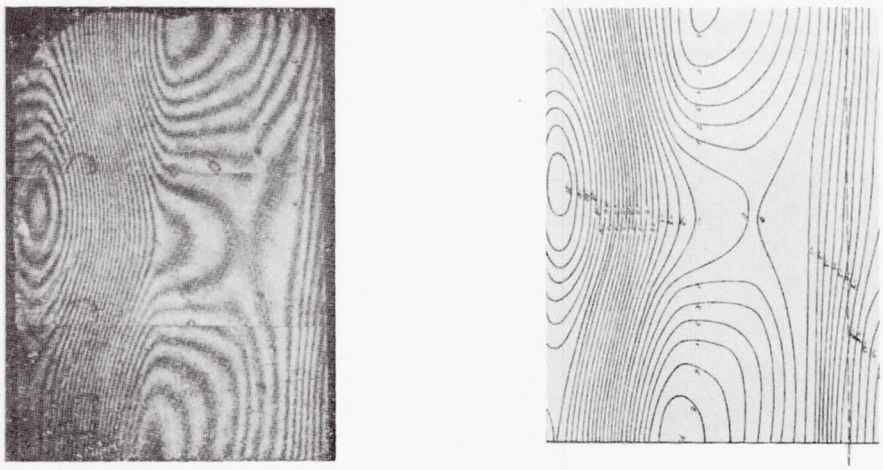

Small object glass

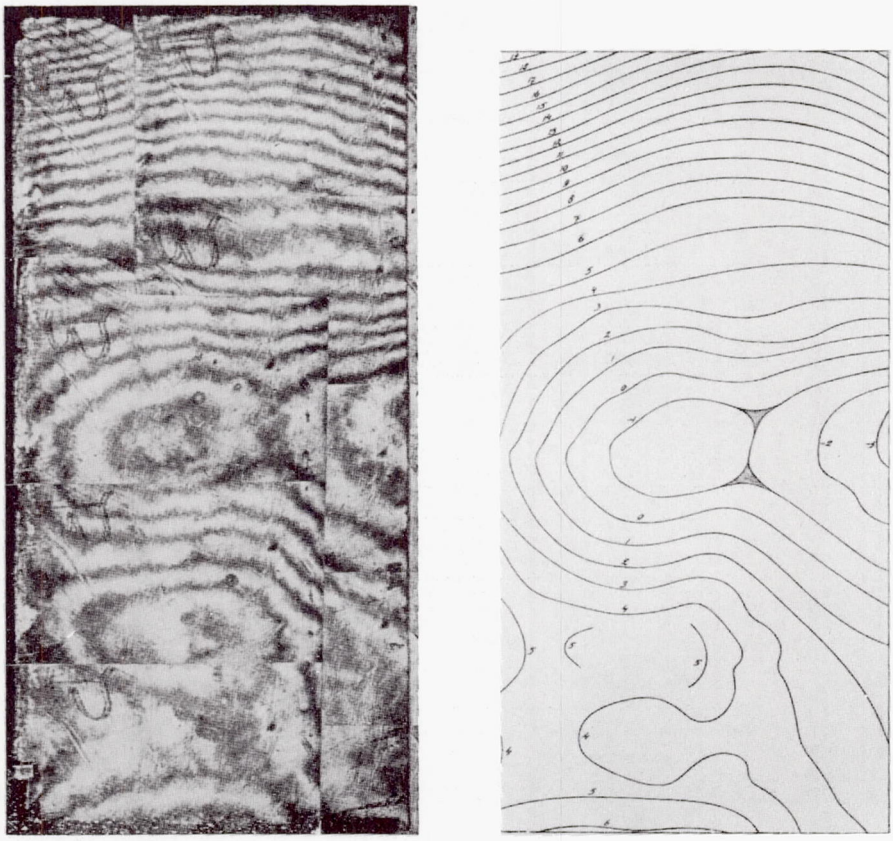

Large object glass

Figure 24.- Evaluated lines of equal density compared with Michelson-interferometer photographs.

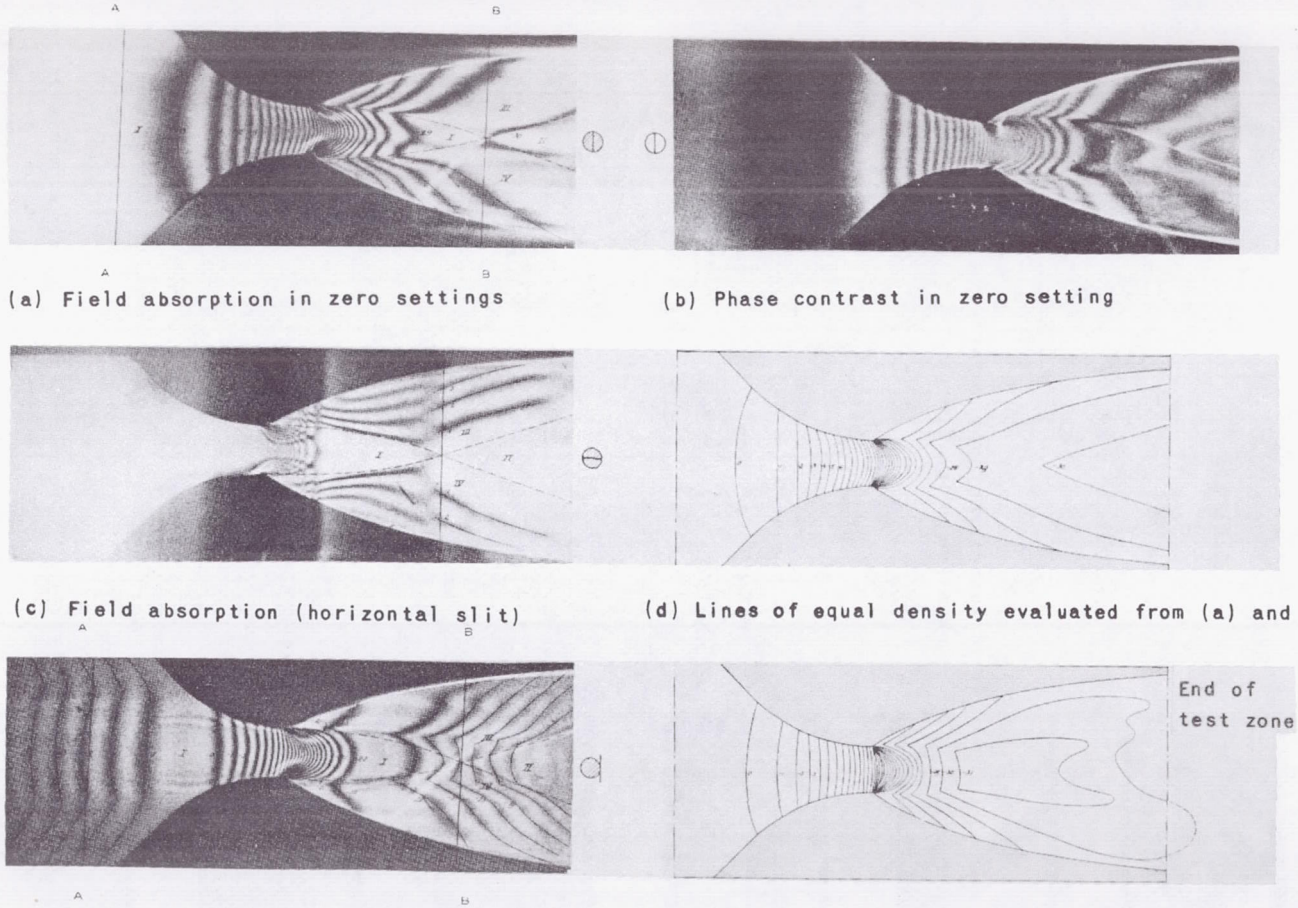

(a) Field absorption in zero settings

(b) Phase contrast in zero setting

(c) Field absorption (horizontal slit)

(d) Lines of equal density evaluated from (a) and (c)

(e) Field absorption with superimposed wedge field

(f) Lines of equal density evaluated from (c) and (e)

Figure 25.- Photographs and evaluation on a Laval nozzle at Ma = 3.0.

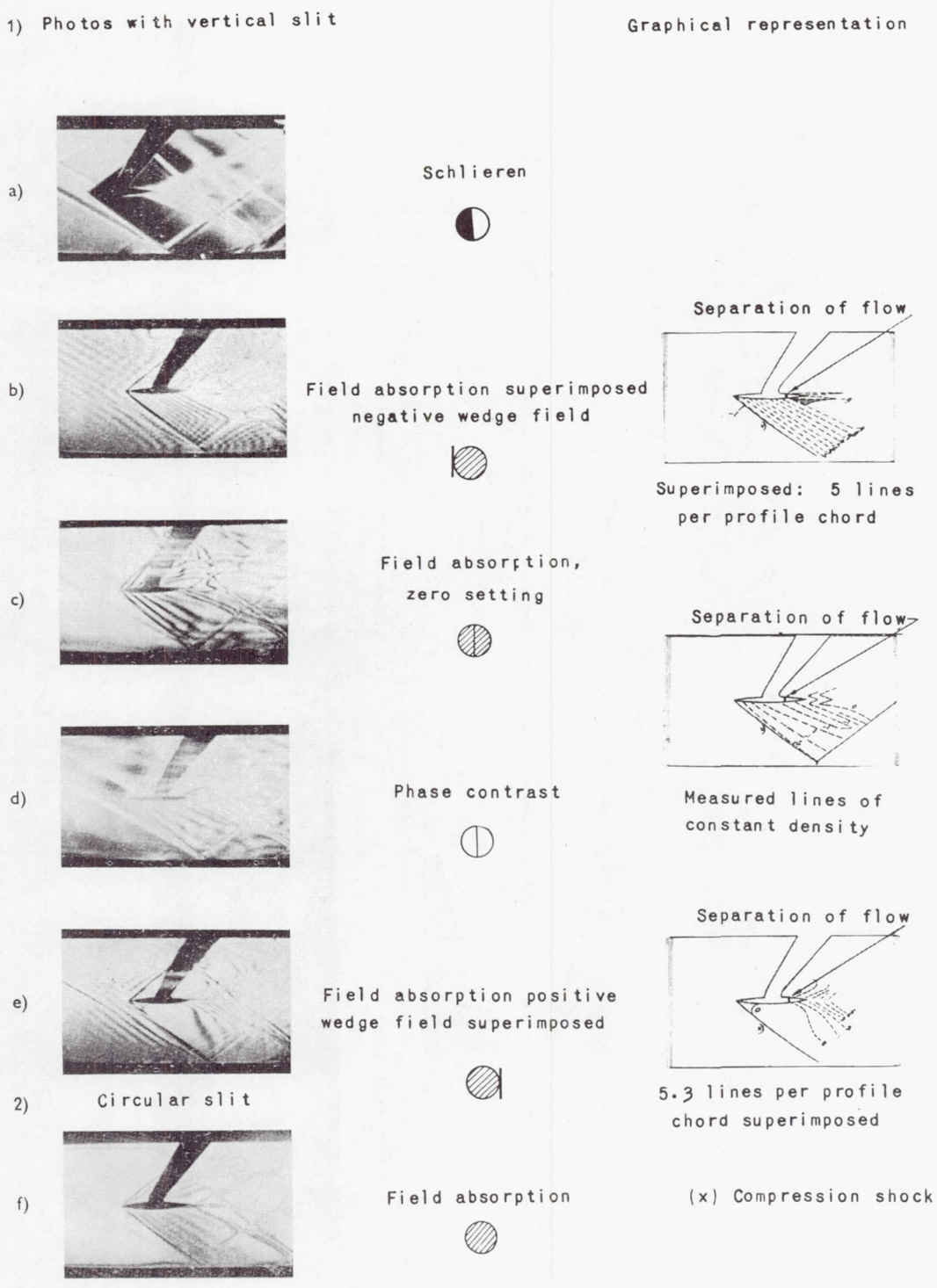

Figure 26.- Variations of the method demonstrated on a supersonic airfoil at Ma = 2.1.

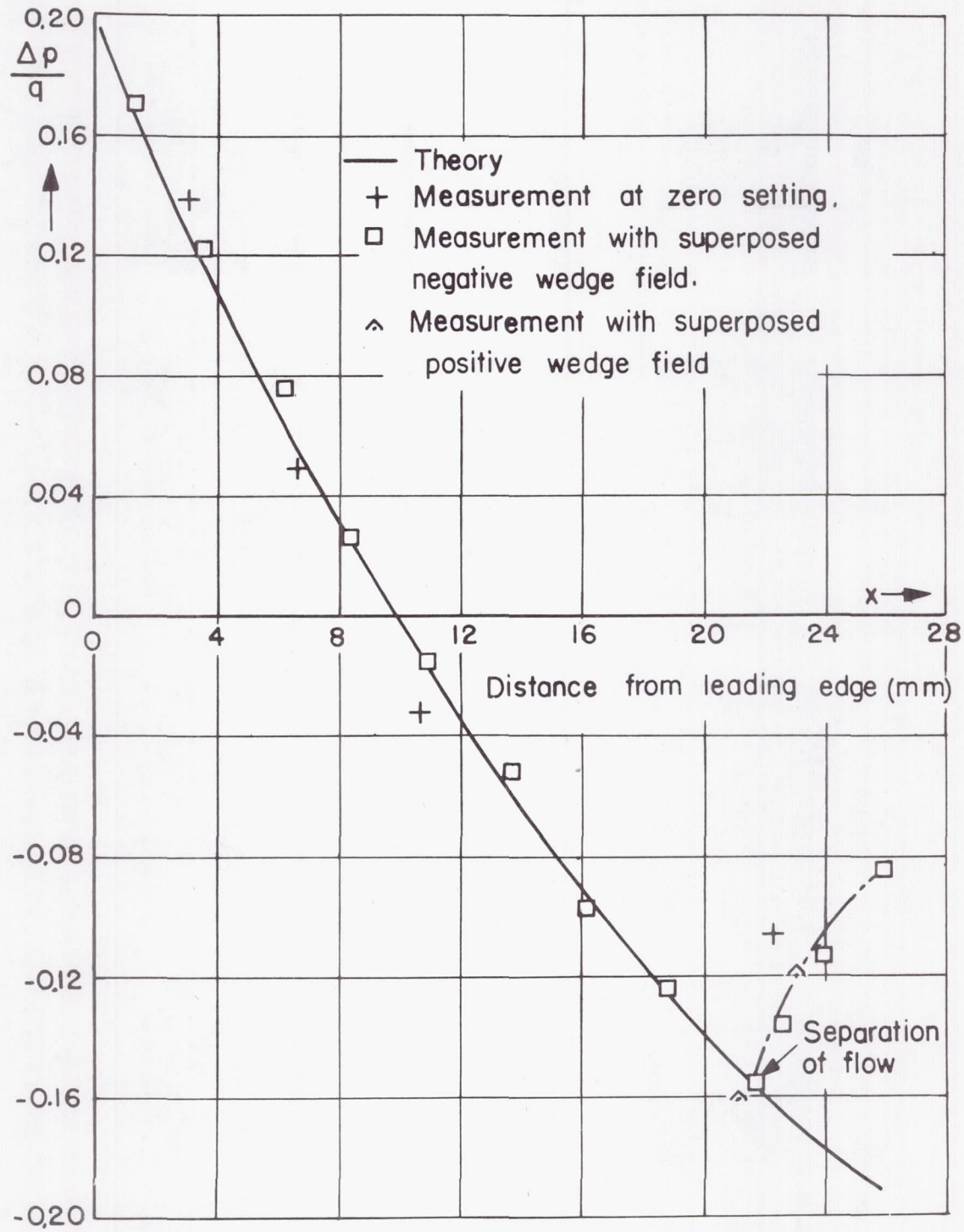

Figure 27.- Pressure distribution on supersonic airfoil at Ma = 2.1.

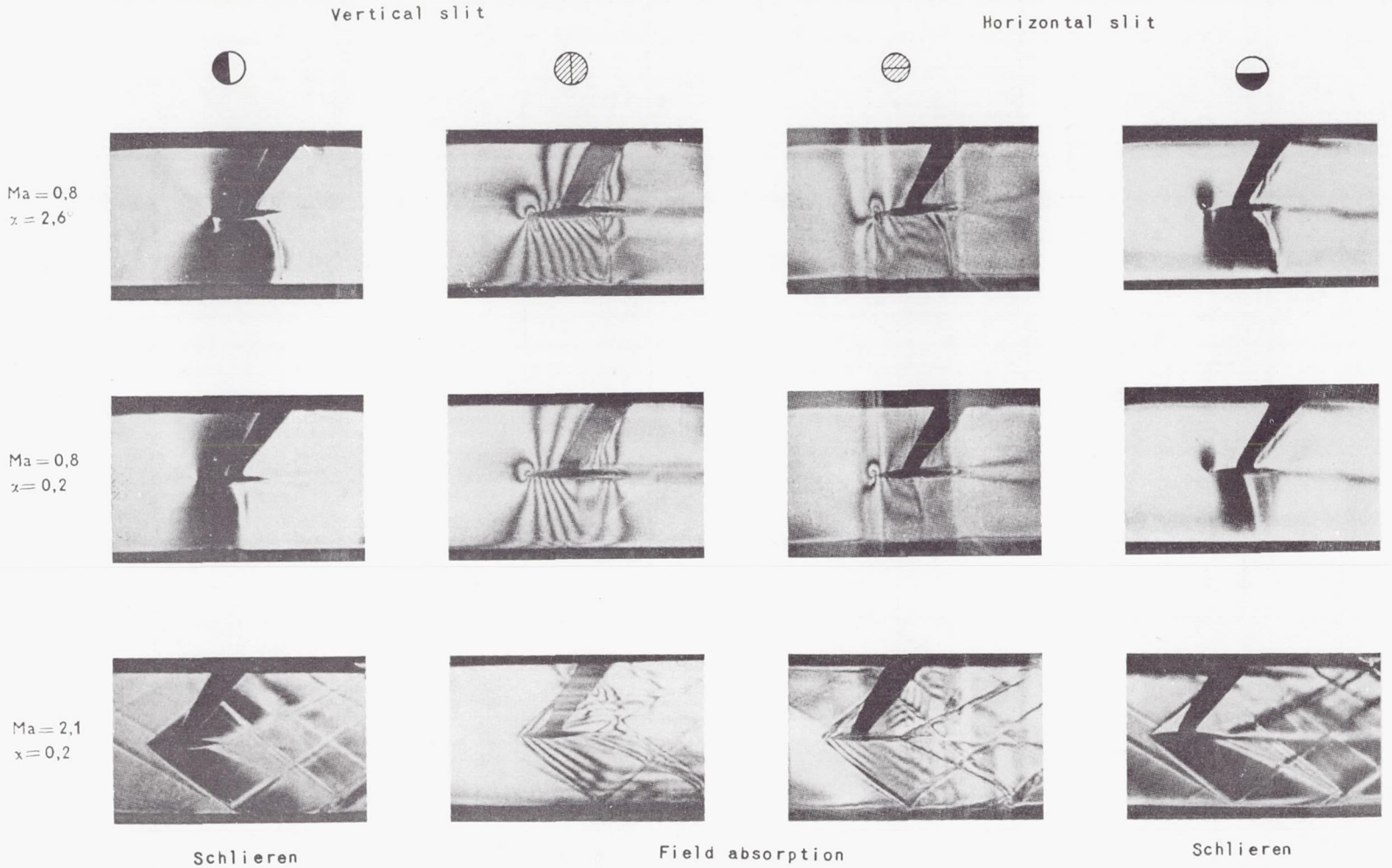

Figure 28.- Examples of complete sets of photographs of interference measurements on airfoils.

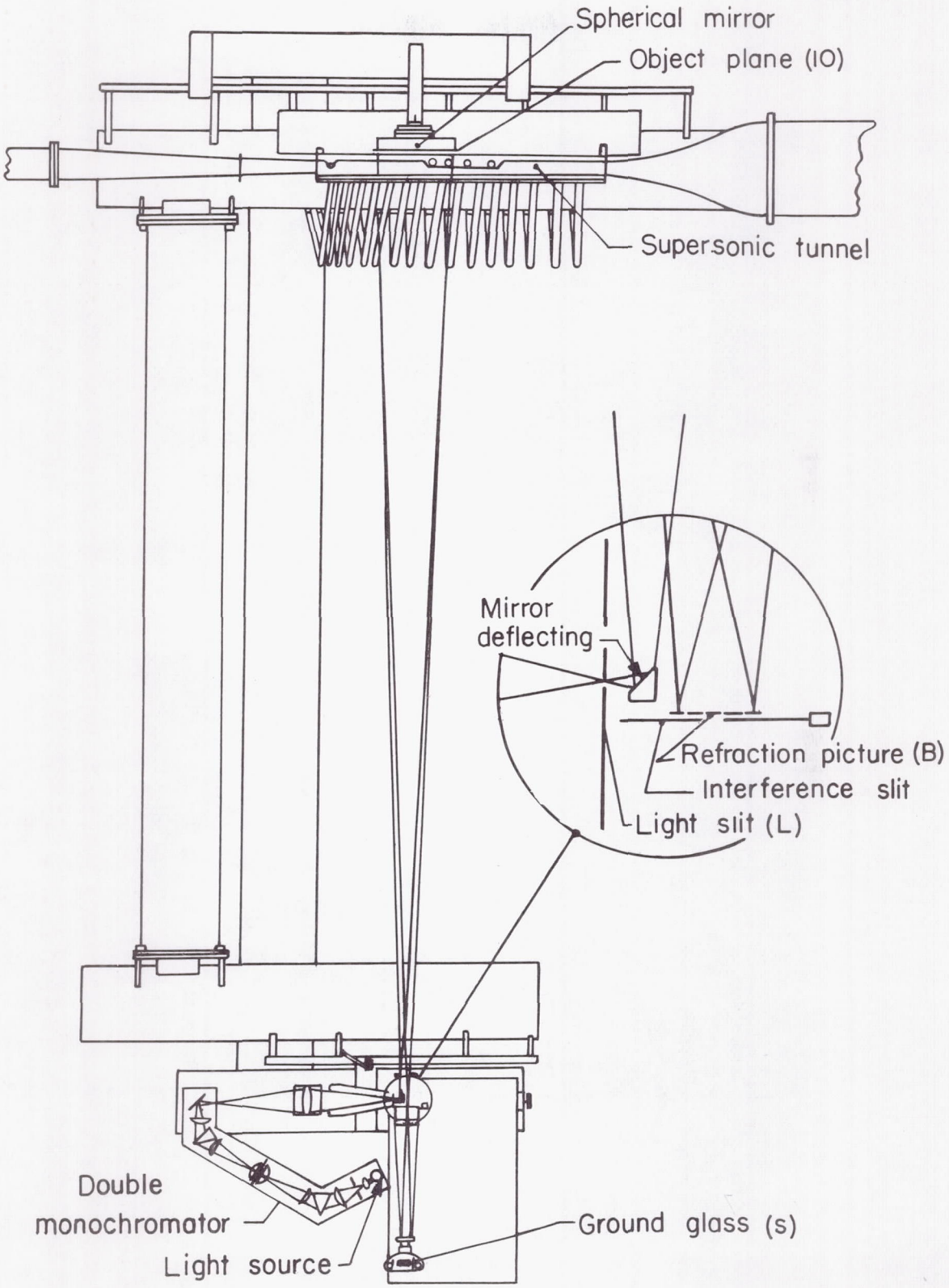

Figure 29.- Experimental setup.

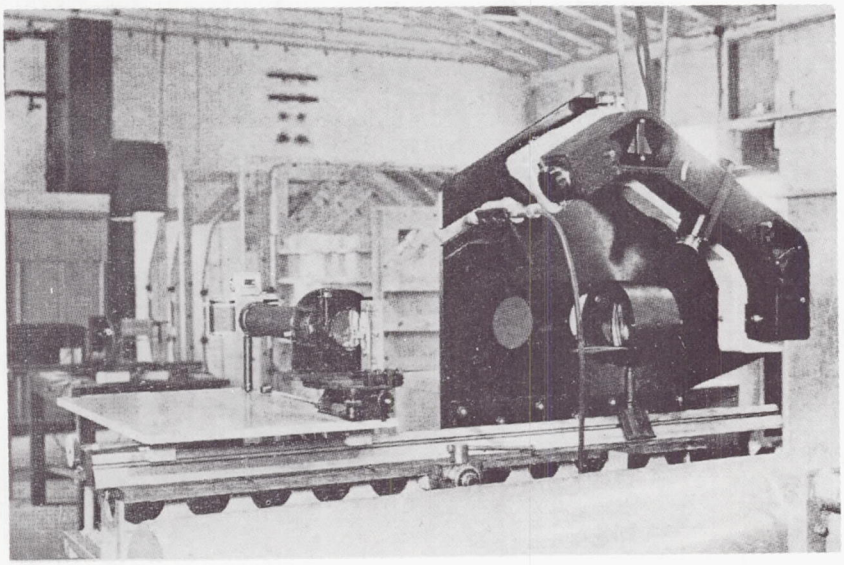

Figure 30.- Optical system.

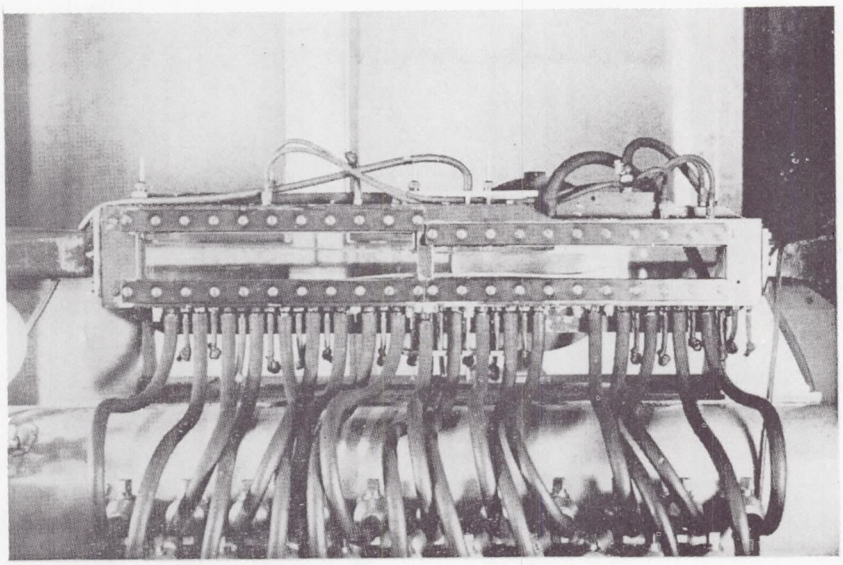

Figure 31.- Supersonic tunnel with mirror in background.

NACA-Langley - 11-16-53 - 1000